Human Molecular Genetics, 2011, Vol. 20, No. 22 ***4475–4490***
doi:10.1093/hmg/ddr380
Advance Access published on August 26, 2011

Impaired motoneuronal retrograde transport in two models of SBMA implicates two sites of androgen action

Michael Q. Kemp[1], Jessica L. Poort[1], Rehan M. Baqri[1], Andrew P. Lieberman[3], S. Marc Breedlove[1,2], Kyle E. Miller[1,4] and Cynthia L. Jordan[1,2,*]

[1]Neuroscience Program and [2]Psychology Department, Michigan State University, 108 Giltner Hall, East Lansing, MI 48824, USA, [3]Department of Pathology, University of Michigan Medical School, 3510 MSRB, 1150 W. Medical Center Dr., Ann Arbor, MI 48109, USA and [4]Department of Zoology, Michigan State University, East Lansing, MI 48824-1115, USA

Received May 2, 2011; Revised and Accepted August 23, 2011

Spinal and bulbar muscular atrophy (SBMA) impairs motor function in men and is linked to a CAG repeat mutation in the *androgen receptor* (*AR*) gene. Defects in motoneuronal retrograde axonal transport may critically mediate motor dysfunction in SBMA, but the site(s) where AR disrupts transport is unknown. We find deficits in retrograde labeling of spinal motoneurons in both a knock-in (KI) and a myogenic transgenic (TG) mouse model of SBMA. Likewise, live imaging of endosomal trafficking in sciatic nerve axons reveals disease-induced deficits in the flux and run length of retrogradely transported endosomes in both KI and TG males, demonstrating that disease triggered in muscle can impair retrograde transport of cargo in motoneuron axons, possibly via defective retrograde signaling. Supporting the idea of impaired retrograde signaling, we find that vascular endothelial growth factor treatment of diseased muscles reverses the transport/trafficking deficit. Transport velocity is also affected in KI males, suggesting a neurogenic component. These results demonstrate that androgens could act via both cell autonomous and non-cell autonomous mechanisms to disrupt axonal transport in motoneurons affected by SBMA.

INTRODUCTION

Defects in axonal transport have been widely implicated in neurodegenerative diseases and may explain the selective vulnerability of long projection neurons, such as motoneurons (1–2). That some neurodegenerative diseases are linked to mutations in trafficking-related proteins argue that this relationship is not merely coincidental. For example, mutations in dynactin 1, part of the molecular machinery mediating retrograde transport (3), may cause some forms of amyotrophic lateral sclerosis (ALS) (4–5). Defects in expression of dynactin 1 expression are also associated with the motoneuron disease spinal and bulbar muscular atrophy (SBMA) (6). Given that there are currently no known cures for either ALS or SBMA, it is crucial to understand the mechanisms regulating axonal transport to suggest new avenues for rescuing motoneurons from disease. Notably, non-cell autonomous mechanisms, which are now recognized as critical determinants of disease susceptibility (7), have largely been unexplored in studies of transport/trafficking defects.

SBMA is a hereditary neuromuscular disease in which lower motoneurons die and muscles atrophy, leading to severe impairment of motor function in men (8). SBMA is linked to a trinucleotide CAG/polyglutamine (polyQ) repeat expansion (>40) in the *androgen receptor* (*AR*) gene (9) and recent evidence indicates that androgens play a crucial role in the pathophysiology of this disease (10–12). Although motoneuron loss is considered a hallmark feature of SBMA, mouse models of SBMA indicate that androgens can trigger motor dysfunction without the loss of motoneurons (13–15). Thus, androgen-dependent cell *dysfunction*, rather than cell *loss*, likely underlies at least early disease pathogenesis in SBMA.

*To whom correspondence should be addressed. Tel: +1 5173551722; Fax: +1 5174322744; Email: jordancy@msu.edu

The SBMA allele of AR has been shown to impair axonal trafficking of anterograde- and/or retrograde-directed cargo (16–18) and may critically underlie motor dysfunction in SBMA, since diseased transgenic (TG) mice expressing a polyQ-expanded (97Q) AR show a marked deficit in retrograde labeling of motoneurons (6). Significantly, this transport deficit emerges early, prior to motor dysfunction, and is associated with deficits in motoneuronal dynactin 1, which is also seen postmortem in spinal motoneurons of humans affected by SBMA, suggesting that defects in retrograde transport in particular may crucially mediate motor dysfunction in SBMA. However, data from a different mouse model of SBMA challenge the idea that axonal transport dysfunction might critically mediate motor dysfunction in SBMA (19). While it is not clear why axonal transport is unperturbed in this other mouse model, deficits in dynactin expression in diseased motoneurons of an SBMA patient suggest that transport should be examined in other available animal models of SBMA.

Because mutant AR is broadly expressed in the 97Q model (14), the site(s) where mutant AR acts to impair retrograde transport remains unknown. While it is clear that mutant AR can act directly in neurons to impair neurons (16–17), AR may also act indirectly, perhaps via their target muscles, to perturb motoneuronal axonal transport. To explore the possibility that such non-cell autonomous mechanisms may affect motoneuronal trafficking in SBMA, we compared retrograde transport in two different mouse models, a knock-in (KI) model of SBMA that expresses a polyQ-expanded AR, under control of the endogenous *AR* promoter, in both motoneurons and muscle (15) and a myogenic mouse model that expresses TG wild-type (WT) AR, *only* in skeletal muscle fibers, yet nonetheless recapitulates many aspects of the SBMA phenotype (20). Most notably, mice in both models exhibit androgen-dependent motor dysfunction, a defining feature of SBMA. While it is still not entirely clear how the polyQ-expanded AR expressed at normal levels and the WT AR expressed at high levels result in strikingly similar pathology, recent data suggest that in both cases, toxicity may arise via abnormal amplification of native AR functions (21).

We now report that diseased mice in both models exhibit striking deficits in the retrograde labeling of motoneurons, comparable to the deficit previously reported for 97Q mice (6). Furthermore, using a novel imaging approach to monitor trafficking endosomes in live axons of the mouse sciatic nerve, we find disease-induced trafficking defects in both models. Intriguingly, endosomal run length is decreased in *both* the KI and myogenic models of SBMA, whereas instantaneous velocity is affected only in KI males, suggesting that cell autonomous and non-cell autonomous mechanisms may act in conjunction to disrupt the motor machinery mediating retrograde axonal transport in SBMA. Supporting the view that non-cell autonomous mechanisms regulate axonal trafficking, we find that delivery of vascular endothelial growth factor (VEGF) to muscle rescues motoneuronal axonal transport deficits from disease, suggesting that muscle-supplied VEGF may have therapeutic value for SBMA.

RESULTS

Diseased motoneurons are slow to accumulate retrogradely transported cholera toxin conjugated to horse radish peroxidase

We began by asking whether affected KI males exhibit a retrograde transport deficit. KI mice express a full-length polyQ-expanded (113Q) AR that is controlled by endogenous AR promoters (15), as in humans with SBMA. We find significant deficits in the muscle strength of adult KI males, based on the hang test (Fig. 1A, $P < 0.0001$, unpaired *t*-test). Because disease progresses at markedly different rates for different KI males, retrograde axonal transport was examined in affected males once their hang time dropped to 60% of controls. The retrograde tracer B subunit of cholera toxin conjugated to horse radish peroxidase (CT-HRP) was injected into the anterior tibialis (AT) muscles of both limbs and 12 h later, the spinal cords of injected mice were harvested, sectioned and reacted to visualize HRP in motoneuronal cell bodies.

The difference was striking, with spinal cord sections of diseased KI males displaying far fewer labeled motoneurons than aged-matched healthy males (Fig. 1B). Counts of the number of retrogradely labeled AT motoneurons confirmed that affected KI males have significantly fewer retrogradely labeled AT motoneurons than WT controls (Fig. 1C, $P < 0.0001$, unpaired *t*-test). To test the possibility that this deficit might due to a loss of motoneurons *per se*, we also counted the total number of motoneurons on one side of the spinal cord through the rostrocaudal extent of the AT motoneurons in an alternate series of HRP-reacted sections counterstained for Nissl. As expected, there were a substantial number of Nissl-stained motoneurons that were not labeled with HRP in diseased KI males (Supplementary Material, Fig. S1). Moreover, motoneuron counts confirmed that diseased KI males have as many motoneurons as healthy WT males, indicating that the deficit in the number of CT-HRP-labeled motoneurons in diseased males reflects a genuine defect in the uptake and/or retrograde delivery of HRP to motoneuronal cell bodies, and not a loss of motoneurons *per se*, consistent with previous reported results (15). However, given the possibility that diseased motoneurons might have smaller cell bodies which could spuriously reduce our detection of HRP-labeled motoneurons, we also measured their cross-sectional area, but found no difference in the size of labeled motoneurons of diseased versus healthy mice (Fig. 1D). Thus, soma size also does not contribute to the deficit in motoneuronal labeling. This evidence from the KI model supports the idea that retrograde axonal transport may be a critical event in SBMA pathogenesis, as was suggested for the 97Q model of SBMA where similar retrograde axonal transport deficits were reported (6). However, for neither of these models is it clear where mutant AR acts to trigger the transport defect. Given that skeletal muscles may indeed play a role in such defects (22), we took advantage of a myogenic TG mouse model in which androgen-dependent disease is triggered via a WT AR transgene expressed only in skeletal muscle fibers (20,23). This model recapitulates the SBMA phenotype found in other SBMA mouse models. Recent evidence also suggests that both the WT and polyQ-expanded AR exert

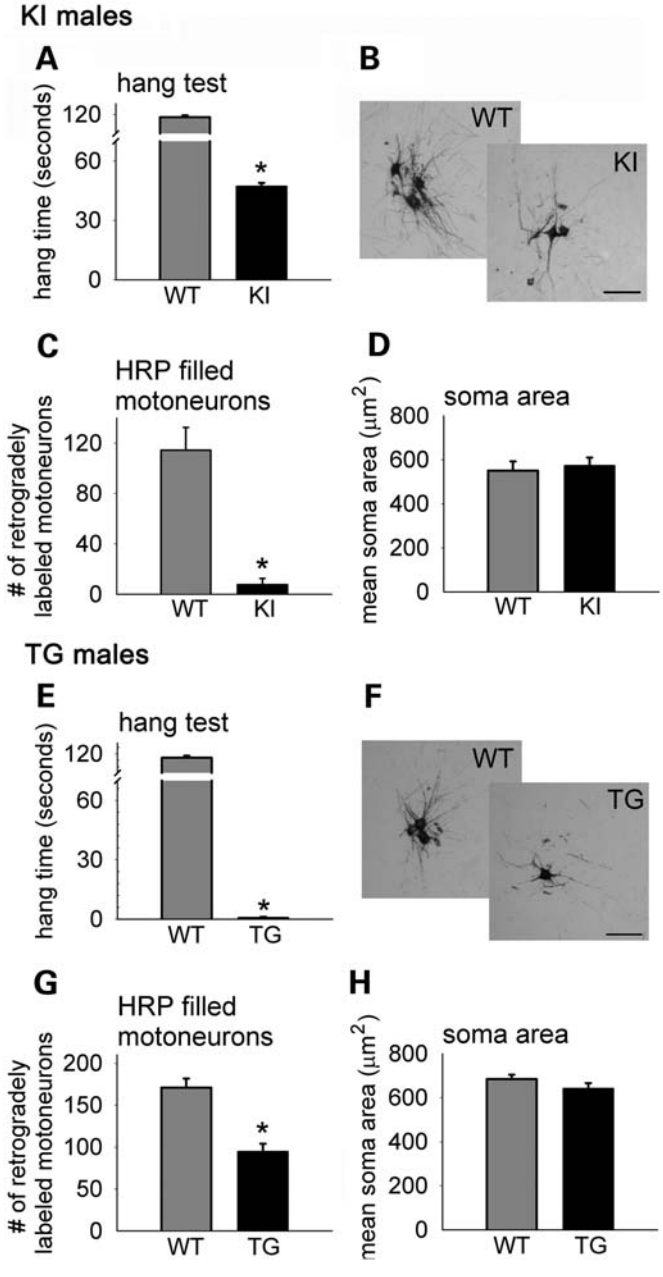

Figure 1. Deficits in motor function and retrograde motoneuronal labeling in diseased male mice of two different SBMA models. (**A**) Male KI SBMA mice expressing a humanized expanded (113) CAG allele of AR driven by the endogenous promoters, as in humans with SBMA, develop significant ($P < 0.0001$) deficits in hang test performance compared with age-matched healthy WT males. (**B** and **C**) Accompanying this motor deficit is a reduction in the retrograde labeling of motoneurons 12 h after CT-HRP is injected into the AT muscle, evident qualitatively in cross-sections of lumbar spinal cord (B). Counts of the number of retrogradely labeled motoneurons confirm that KI males have significantly fewer ($P < 0.0001$) labeled AT motoneurons than WT males (C). Unilateral counts of the total number of Nissl-stained motoneurons spanning the rostrocaudal extent of AT motoneurons indicate that KI and WT males have comparable numbers of motoneurons (Supplementary Material, Fig. S1) and suggest that the retrograde labeling deficit reflects impaired uptake and/or retrograde transport and not cell loss. (**D**) Average size of labeled motoneuronal cell bodies is comparable in KI and WT males, indicating that reduced cell size also cannot account for the decreased number of retrogradely labeled motoneurons detected in diseased KI males. (**E**–**G**) Diseased TG males over-expressing a WT rat AR allele selectively in muscle fibers also show marked deficits in muscle strength based on hang test performance ($P < 0.0001$) and fewer ($P = 0.0003$) retrogradely labeled motoneurons compared with WT males (F and G), suggesting that uptake and/or retrograde transport is also disrupted in myogenic-diseased TG males. (**H**) Cross-sectional area of labeled motoneuronal cell bodies is comparable in TG and WT males, indicating that cell atrophy cannot explain the fewer number of labeled motoneurons observed in diseased TG males. Scale bar = 100 μm. Graphs represent mean ± SEM of $N = 6$ per group. *Significant differences between groups based on unpaired *t*-tests.

toxicity through comparable molecular mechanisms (21), reinforcing the heuristic value of the myogenic model. Furthermore, the myogenic model offers the unique advantage of revealing whether expression of AR in muscle fibers alone can impart disease to motoneurons that do not themselves express the disease allele.

Adult TG males with severe muscle weakness (Fig. 1E, $P < 0.0001$, unpaired *t*-test) also show a marked deficit in retrograde labeling of AT motoneurons (Fig. 1F and G). Twelve hours after injection of CT-HRP into AT muscles, affected TG males have approximately half the number of HRP-labeled motoneurons as healthy, aged-matched WT males ($P = 0.0003$, unpaired *t*-test). Both diseased TG and healthy WT males have the same size motoneurons (Fig. 1H), ruling out any potential contribution of soma size. Moreover, previous cell counts performed in Nissl-stained material indicate that severely affected TG males nonetheless have a normal number of lumbar motoneurons (20).

There are two notable differences in retrograde labeling in the two disease models. First, the average number of retrogradely labeled AT motoneurons is lower in WT controls of the KI model compared with WT controls of the myogenic model (~114 versus ~171, respectively). This difference may be due to the two different genetic backgrounds: 129 for the KI model and C57Bl/6J for the myogenic model and underscores the importance of using appropriately matched WT controls in such studies. We also find that affected KI males show a deficit in retrograde labeling that is more severe than in TG mice, with nearly a 15-fold deficit for KI males compared with about a 2-fold deficit for diseased myogenic mice. Given that mutant AR is expressed in many cell types in the KI model, including motoneurons and muscle fibers, the greater transport deficit exhibited by KI males may reflect the combined impact of AR acting in multiple cell types, via both cell autonomous and non-cell autonomous mechanisms, whereas only non-cell autonomous mechanisms can influence retrograde transport in motoneurons of the myogenic model. It is also possible that transport is more severely affected in the KI model because the expanded glutamine tract in AR exerts a greater effect on this process. However, whether this greater toxicity of AR on retrograde transport in the KI model is relevant to motor dysfunction is unclear, given that mice in the myogenic model show a greater disruption of motor function, yet a milder disruption of axonal transport than KI males. Possible explanations for this apparent incongruence include that overexpression of WT AR in muscle disrupts muscle function, independent of its effects on axonal transport and that both contribute to the more profound impairment of motor function in the myogenic model, or that mutant AR acting in multiple cell types disrupt

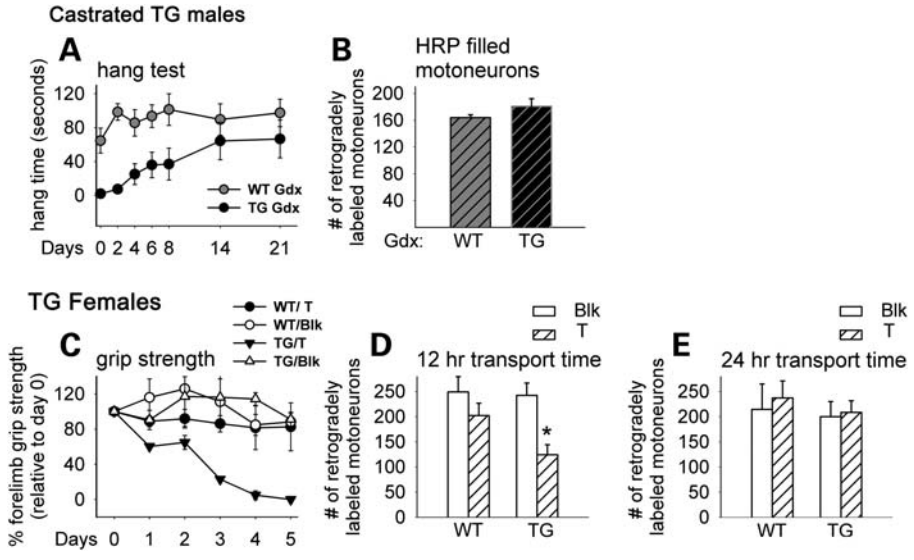

Figure 2. Deficit in retrograde motoneuronal labeling is androgen-dependent and correlates with changes in motor function in myogenic-affected mice after 12 h of transport. (**A** and **B**) Gonadectomy (Gdx) of adult, chronically diseased TG males eliminates the deficit in both muscle strength and retrograde labeling. Castrated TG males steadily recover muscle strength (A), increasing their hang times to that of castrated WT males 14 and 21 days after castration. Comparable recovery of muscle strength was also detected based on the grip strength test (data not shown). At 21 days after castration, the deficit in retrogradely labeled motoneurons is also eliminated, with the number of labeled AT motoneurons in TG males increased to match that of their WT brothers. Note that castration had no effect on the number of retrogradely labeled motoneurons in WT males (B, compare to Fig. 1G). Evidently, once gonadal androgens are removed, CT-HRP is taken up and transported with the same efficiency in adult TG and WT males, ruling out the possibility that fewer total motoneurons accounts for the labeling deficit in TG males before castration (Fig. 1 F–G). (**C**–**E**) Acute androgen treatment of adult asymptomatic TG females induces the *same* deficit in motor function and retrograde transport as seen in adult TG males. Forelimb grip strength in TG females drops significantly within 24 h of exposure to exogenous testosterone (T) (comparison of TG/T day 0 to day 1, $P = 0.0312$) and reaches basement by day 5 (C). TG females treated with T for 5 days also have significantly fewer retrogradely labeled AT motoneurons after 12 h of transport compared with controls (TG/T versus TG/Blk: $P < 0.003$, indicated by asterisk, D). Significantly, when transport time after CT-HRP injection is extended to 24 h (E), the labeling deficit is eliminated in diseased (T-treated) TG females. Note that a longer transport time increases the number of retrogradely labeled motoneurons only in T-treated TG females that have compromised motor function, suggesting that diseased motoneurons are slow to accumulate CT-HRP in their cell bodies compared with non-diseased motoneurons. These data also argue that cell loss cannot account for the retrograde labeling deficit in TG animals. Graphs represent mean ± SEM (Ns = 6/group) with significant group differences determined by a paired *t*-test (B) or two- or three-way ANOVAs followed by PLSD (A, C–E).

aspects of axonal transport that do not underlie motor dysfunction.

However, given that diseased TG males have fewer motor axons (20), it was possible that a deficit in axon number caused the reduced retrograde labeling in the myogenic model (20). We examined this possibility by gonadectomizing (Gdx) chronically diseased males, and found that castration of TG mice not only reversed the deficit in muscle strength (Fig. 2A, WT Gdx versus TG Gdx at days 14 and 21, $P > 0.05$), as previously reported (20), but also eliminated the deficit in retrograde labeling (Fig. 2B). These data argue that the deficit in transport exhibited by gonadally intact TG males is not caused by a loss of axons.

We also examined retrograde transport of CT-HRP in adult TG females in which disease is rapidly and robustly triggered by testosterone (T) treatment. Such T treatment results in circulating T levels that are somewhat below normal adult males (24). TG females in our myogenic model offer a unique opportunity for dissociating primary mechanisms from secondary effects of chronic disease because TG females acutely express disease symptoms *only* when exposed to male levels of androgens and do so without motor axon loss (20,23).

Because untreated adult TG females have normal motor function, we first confirmed the effects of T on motor function. Replicating previous findings (20), 5 days of T treatment lead to a devastating loss of motor function for TG females, shown by a loss of grip strength (Fig. 2C, TG/T day 0 versus day 5: $P < 0.0001$). Such T treatment also induces a robust labeling deficit in these same females, detected 12 h after CT-HRP was injected into their AT muscles [Fig. 2D; significant main effect of treatment: $P = 0.0035$, based on a two-way analysis of variance (ANOVA)]. *Post hoc* comparisons indicate that such symptomatic T-treated TG females have significantly fewer retrogradely labeled AT motoneurons than asymptomatic blank-treated TG controls ($P < 0.003$), while none of the three control groups differs from one another (ps = 0.205–0.854). Thus, it is only the combination of expressing an AR transgene in skeletal muscle fibers and male levels of androgens that induce the loss of motor function *and* the transport defect. Motoneuronal soma size in diseased TG females is not significantly different from the other three control groups (data not shown). We also find that extending transport time from 12 to 24 h eliminated the labeling deficit by increasing the number of retrogradely labeled motoneurons in motor-impaired TG females (Fig. 2E). These data confirm that TG and WT females have equivalent *numbers* of motoneurons innervating the AT muscle, consistent with previous results (24) and indicate that diseased AT motoneurons are *slower* to accumulate CT-HRP in their cell bodies.

Diseased mice show deficits in axonal trafficking of endosomes

Two possible explanations for why diseased motoneurons are slow to accumulate CT-HRP in their cell bodies include (1) fewer endosomes moving along axons, possibly because of defects in the uptake/early vesicular trafficking of CT in motor nerve terminals, and/or (2) endosomes move more slowly along axons, possibly reflecting defects in the dynein/dynactin motor complex mediating retrograde axonal transport. To assess whether these changes underlie the deficit in motoneuronal labeling in the spinal cord, we adapted a live imaging approach (25–27) in which the B subunit of cholera toxin conjugated to the fluorescent tag Alexa Fluor 488 (CT-AF_{488}) was injected into the AT and gastrocnemius muscles to label retrogradely trafficking endosomes in the sciatic nerve. At later time points, transport of labeled vesicles was observed in sciatic nerve explants using confocal microscopy. This approach allows us to directly monitor endosomal trafficking in sciatic nerve axons of diseased and healthy mice minutes after the nerve is harvested from living animals and sheds light on whether defects originating in the synapse and/or axon likely contribute to the labeling deficit of spinal motoneurons.

Before we assessed the effects of disease on endosomal trafficking, we carried out a number of experiments to validate this novel preparation. We first confirmed that moving fluorescent profiles are evident only in sciatic nerve explants when CT-AF_{488} was injected into muscle. We also varied the time between tracer injection and nerve harvest (i.e. transport time) and find that 4 h yielded the maximum number of trafficking endosomes moving in a retrograde direction, consistent with the established velocity of retrograde transport (26–28).

The stability of endosomal trafficking in explants was also determined by recording beyond the standard 30 min recording window. We find that neither flux nor net velocity of trafficking endosomes change significantly over time (Supplementary Material, Fig. S2A and B), even when recordings were extended beyond an hour, in good agreement with previous results demonstrating stable vesicular trafficking $\geq$3 h in comparable sciatic nerve explants (27). Such control experiments also confirmed stable endosomal trafficking in axons of explanted nerve from diseased mice (Supplementary Material, Fig. S2A and B).

Finally, we sought to verify that the transport of CT-AF_{488}-labeled endosomes in sciatic nerve axons is microtubule-dependent. Nocodazole (25 μg per muscle), an agent that perturbs microtubule polymerization, was injected intramuscularly in WT males 10 h before injection of CT-AF_{488}. This dose essentially blocked endosomal trafficking on the side exposed to nocodazole, whereas endosomal trafficking was unimpaired on the vehicle-treated side. Halving the dose of nocodazole (12.5 μg per muscle) resulted in oscillating endosomes, while one-fourth the original dose (6.25 μg per muscle) allowed sufficient endosomal trafficking to quantitatively assess net velocity and flux. This dose of nocodazole resulted in significantly fewer trafficking endosomes, which traveled at a modestly (13%) slower rate (Supplementary Material, Fig. S2C and D). These results confirm that retrograde trafficking of CT-AF_{488}-labeled endosomes in living axons of sciatic nerve explants is a microtubule-dependent process as expected (26). All together, these data indicate that our method for assessing retrograde trafficking of endosomes in sciatic nerve axons of diseased and healthy mice is a reliable and valid assay.

To evaluate how disease might affect endosomal trafficking, we initially focused on two main measures, flux and net velocity. Endosomal flux is the number of endosomes that traverse past an arbitrarily defined point in the axon over time, whereas net velocity is the net distance traveled by an endosome over time, a measure that can include stalls and reversals. Both measures are readily obtained from a kymograph (Fig. 3A) which shows the movement of individual CT-AF_{488}-labeled profiles within a single axon over time and space. Given that endosomal flux is the sum result of a number of endocytotic and trafficking events beginning with uptake of CT by nerve terminals, whereas endosomal net velocity reflects the efficiency by which endosomes transport retrogradely along axons, these two measures combined begin to delineate what aspects of the endocytotic/trafficking machinery are perturbed by disease.

We find that endosomal trafficking is severely impaired in KI males, paralleling the rather severe effect on retrograde labeling (Fig. 1). The most obvious deficit is a marked depletion in the number of retrogradely transporting endosomes over time (i.e. flux), apparent even during live imaging (see Supplementary Material, Movie S1 and Fig. S3). Quantitative analysis of retrogradely transporting endosomes from kymographs confirmed this impression, revealing a significant 5-fold decrease in endosomal flux (Fig. 3B, $P < 0.0001$, unpaired *t*-test). We also find a significant decrease in the net velocity of trafficking endosomes in affected KI males (Fig. 3C, $P = 0.0254$, unpaired *t*-test). In sum, peripheral axons of diseased KI males contain fewer moving endosomes, which travel a net distance more slowly than those of healthy mice, and suggest that perturbations in both the dynein/dynactin motor complex, mediating retrograde transport along axons, and earlier endocytotic trafficking events in the synapse may contribute to the profound labeling deficit of motoneuronal cell bodies in KI males. Importantly, we find no evidence of decline in endosomal trafficking across the two bouts of recording from the same nerve explants (Supplementary Material, Fig. S4A and B). If anything, endosomal flux and net velocity are slightly higher in the second video than in the first, suggesting that the deficits in endosomal flux and net velocity likely reflect genuine trafficking defects *in vivo*. Thus, data from the KI model reinforce the idea that SBMA may involve defects in retrograde axonal transport. However, because the KI model provides no information about where mutant AR acts to instigate these changes, we next examined endosomal trafficking in the myogenic model of SBMA in which androgens act via ARs in skeletal muscle fibers to trigger a retrograde labeling deficit in motoneurons (Fig. 1G).

Using the same live imaging approach, we find that sciatic nerve axons of diseased TG males also exhibit a significant, though milder, deficit in endosomal flux than do KI males, with axons of motor-impaired TG males containing about half the number of trafficking endosomes as healthy WT brothers (Fig. 3D, $P < 0.0001$, unpaired *t*-test). Notably, *net velocity is normal* in diseased TG males (Fig. 3E, see also Supplementary Material, Movie S2). These results suggest that

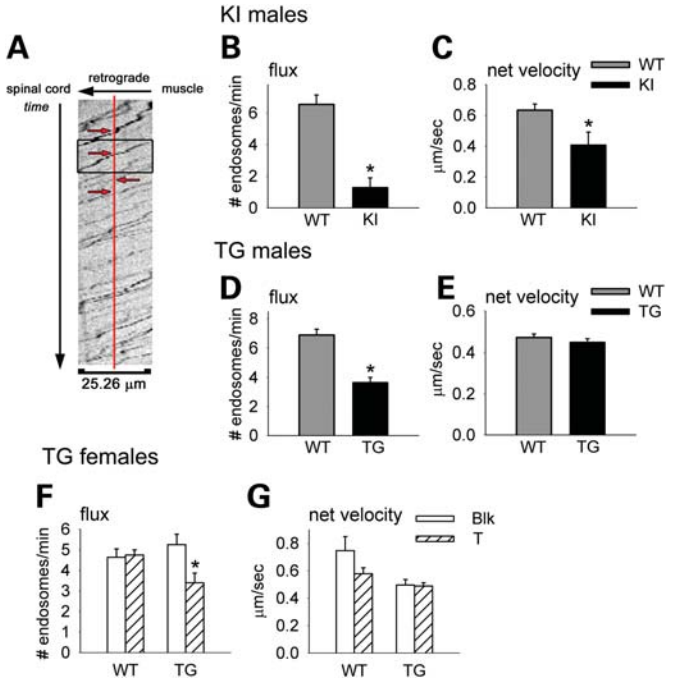

Figure 3. Defects in endosomal trafficking in sciatic nerve axons of motor-impaired KI and myogenic TG mice. (**A**) Representative kymograph from live video imaging of cholera toxin-AlexaFluor 488 (CT-AF_{488}) labeled endosomes show multiple endosomal traces (positively sloped black lines, red arrows pointing to some) in a single axon, reflecting the retrograde movement of labeled endosomes over time (vertical plane) and distance (horizontal plane). We measured endosomal flux and velocity from such kymographs. Endosomal flux is the number of endosomes that cross a point in the axon (indicated by the red vertical line) over time, whereas endosomal net velocity is the net retrograde distance traveled over time (indicated by the black rectangle for one endosomal trace). (**B** and **C**) Quantitative analysis of such kymographs indicates that diseased KI males exhibit significant deficits in both endosomal flux ($P < 0.0001$) and net velocity ($P = 0.0254$) compared with WT males, suggesting that impairments in both the number and speed of retrogradely trafficking endosomes in sciatic nerve underlie the marked deficit in retrograde labeling of diseased motoneurons in the KI model (Fig. 1C). Endosomal flux and net velocity are also comparable from the two videos taken consecutively from the same set of nerve explants (see Supplementary Material, Fig. S4A and B), arguing that the deficits in endosomal flux and net velocity in diseased axons from KI mice do not reflect a deterioration of diseased explants *ex vivo*. (**D** and **E**). Unlike KI males, sciatic nerve axons from chronically diseased TG males exhibit a significant reduction only in endosomal flux compared with unaffected WT controls ($P < 0.0001$), with no deficit in net velocity. The selective effect on endosomal flux in this model also suggests a genuine trafficking defect *in vivo* which is not caused by deterioration. Moreover, we saw comparable stability across consecutive recordings from the same axons of TG males (see Supplementary Material, Fig. S4C and D). (**F** and **G**) TG females treated with T for 5 days show the same disease-related deficit in endosomal flux without a change in velocity as do chronically diseased males, indicating that acute exposure to T is sufficient to induce a comparable deficit in endosomal flux. Because the disease-causing AR allele in KI mice is expressed in both motoneurons and muscles, but only in muscle fibers of TG mice, these data raise the intriguing possibility that AR toxicity originating in motoneurons and muscle impair distinct trafficking mechanisms underlying endosomal flux and velocity. Graphs represent mean ± SEM (Ns = 4–6/group for B–E and 6/group for F–K) with significant group differences based on unpaired *t*-tests for studies on males and two-way ANOVAs followed by PLSD for the study on females.

HRP accumulates more slowly in motoneurons of diseased myogenic mice because fewer endosomes are transported retrogradely, implicating problems originating in the synapse prior to axonal transport. The selective effect of disease on endosomal flux also indicates that the deficit is not due to general deterioration of diseased nerve explants. Finding the same pattern of results in each of the two consecutive videos without evidence of decline (Supplementary Material, Fig. S4C and D) further supports this view.

We also examined endosomal trafficking in adult TG females that become symptomatic *only* when treated with androgens, and find a comparable deficit in endosomal flux as found in chronically diseased TG males (Fig. 3F). Also like TG males, net velocity is not affected in motor-impaired TG females (Fig. 3G). Because T treatment reduces flux only in TG females ($P < 0.03$ compared with control-treated TGs), there is a significant interaction of treatment with genotype ($P = 0.0289$, two-way ANOVA) on endosomal flux. Neither TG AR nor androgen treatment alone affects endosomal flux. No statistically significant effects were found on net velocity. We again find no evidence of decline in endosomal trafficking across the two consecutive recordings done on the same nerve explants (data not shown). These data indicate that AR acts in muscle of diseased myogenic mice to reduce the number, and thus flux, but not net velocity, of retrogradely transported CT-containing endosomes. Data from the KI and myogenic models of SBMA together show that AR can act via two different cell types (motoneurons versus muscle fibers) to perturb two different trafficking parameters, acting in a cell autonomous manner in motoneurons to affect the *speed* at which endosomes traffic retrogradely in axons, and in a non-cell autonomous manner in muscle fibers to affect the *number* of endosomes that traffic retrogradely, with each contributing to a labeling deficit in motoneuronal cell bodies.

Denervation or reduced size of neuromuscular junctions (NMJs) cannot account for the deficit in endosomal flux

One scenario that could explain the deficit in endosomal flux is retraction of nerve terminals from muscle, effectively reducing the amount of CT transported along axons. Synaptic retraction is also suggested by the denervation-like changes in gene expression in muscles of diseased KI and TG males (15,20). Hence, we examined neuromuscular junctions (NMJs) in AT muscles for evidence of denervation. We also measured the size of synapses since reduced overall size might also contribute to the reduced endosomal flux and labeling deficit in diseased mice.

We find no morphological evidence indicating that disease triggers denervation of muscle fibers in either KI or myogenic models of SBMA (Fig. 4A and B). Every motor endplate examined in AT muscles of diseased KI and TG males was fully contacted by a motor nerve terminal, and lacked exposed areas suggestive of ongoing denervation. While NMJs in TG males look pathological (Fig. 4B), appearing more fragmented than normal, NMJs in KI males look remarkably normal (Fig. 4A) with the exception that many show a marked increase in the intensity of synaptophysin staining (data not shown), possibly reflecting accumulated synaptic vesicles in nerve terminals. Junctions of KI males are normal in size [333.62 ± 16.10 (WT, $N = 5$) versus 297.88 ± 19.07 (KI, $N = 6$)]. Diseased myogenic males, on the other hand, have significantly smaller junctions than normal [354.43 ± 16.58 (mean ± SEM; WT)

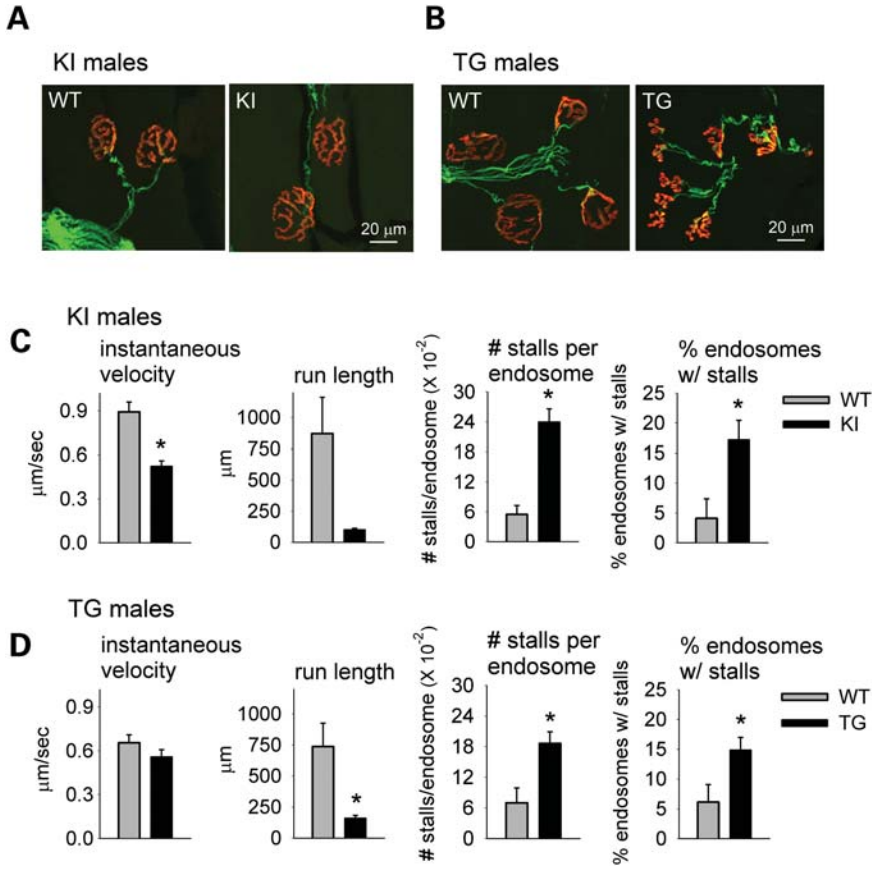

Figure 4. NMJs of diseased mice are intact, but diseased KI and myogenic mice show other trafficking defects, including reduced endosomal run lengths. (**A** and **B**) Overlay of confocal images of presynaptic motor axons and terminals (green) and their underlying postsynaptic AChRs (red) in diseased AT muscles of KI (A) and TG (B) males reveal precise alignment of pre- and postsynaptic elements of the NMJ, suggesting that denervation of NMJs cannot explain the deficit in endosomal flux evident in both models. Even though junctions appear structurally intact, these data do not rule out the possibility that junctions are functionally denervated. While junctional fragmentation in diseased TG males could potentially contribute to the flux deficit in the myogenic model, the NMJs of diseased TG females appear normal, without fragmentation (data not shown), arguing against this possibility. (**C** and **D**) More detailed analyses of kymographs from KI (C) and TG (D) males indicate that instantaneous velocity of moving endosomes is significantly reduced in KI males, but not in TG males, compared with their respective WT controls, potentially explaining why net velocity is reduced only in KI males. In contrast, diseased males in both models show reduced endosomal run length, associated with significant increases in the number of stalls per endosome and the proportion of endosomes that stall (see also Supplementary Material, Movies S1 and S2). The similar disruption of retrograde trafficking in these two models, which display identical motor dysfunction, is consistent with the possibility that defects in the motor machinery mediating retrograde trafficking of cargo along axons may critically underlie motor dysfunction in SBMA (6). Moreover, data from the myogenic model argue that skeletal muscles can impart such transport dysfunctions in motoneurons. Graphs represent mean ± SEM of N = number of mice/group (Ns reported in Fig. 3). *Significantly different than WT controls based on unpaired t-tests.

versus 171.93 ± 5.13 (TG), $N = 3$ per group]. Given the possibility that reduced junctional size contributes to the endosomal flux deficit in the myogenic model, we measured the size of junctions in acutely diseased TG females, which exhibit a comparable retrograde labeling and flux deficit as chronically diseased myogenic males. In contrast to chronically diseased males, the size of junctions in diseased TG females is unaffected [318.39 ± 50.17 (control-treated TGs) versus 327.00 ± 36.72 (T-treated TGs); $N = 3$ per group]. Thus, neither denervation nor reduced endplate size explains why diseased KI or myogenic SBMA mice exhibit deficits in endosomal flux.

Endosomes have shorter run lengths in diseased KI and myogenic males

To explore potential mechanisms underlying the decreased net velocity of CT-AF_{488}-labeled endosomes in KI males, we examined other trafficking parameters, including instantaneous velocity and run length. Instantaneous velocity of endosomes reflects the absolute speed of retrogradely directed endosomes minus any stalls and/or reversals that interrupt the smooth retrograde transport of endosomes along axons. The more stalls an endosome exhibits, the shorter the run length. Estimates of instantaneous velocity and run length of labeled endosomes from the kymographs indicate that both trafficking measures are reduced in KI males compared with WT controls (Fig. 4C; instantaneous velocity: $P < 0.004$, see also Supplementary Material, Fig. S3), although the reduced run length falls short of significance ($P = 0.068$), probably because of the large error variance in WTs. When we determined the number of stalls per endosome and the proportion of endosomes that stall, we find that both are significantly increased in KI males ($P < 0.001$ for both), suggesting a genuine decrease in run length in diseased motor axons of KI males. A comparable analysis of kymographs from diseased myogenic males revealed surprisingly some of the same trafficking defects as KI males

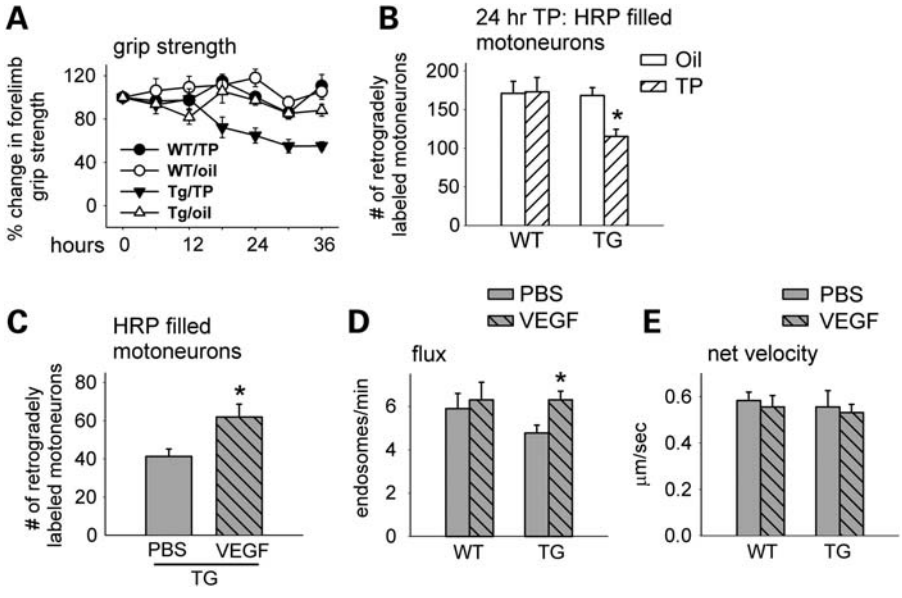

Figure 5. Exogenous VEGF reverses early deficits in retrograde labeling of motoneurons and endosomal flux. (**A**) Systemic exposure via s.c. injection of testosterone propionate (TP) leads to a rapid and significant loss in the grip strength of TG females within 18 h ($P < 0.006$, compared to time 0). (**B**) After 24 h of TP exposure, CT-HRP injected into the AT muscle of such motor-impaired TG females reveals a significant and selective deficit in the number of AT motoneurons containing retrogradely transported label after 12 h of transport ($P < 0.02$ for both, compared with oil-treated TG or TP-treated WT females). (**C**) Locally treating AT on one side of TP-treated TG females with VEGF increases the number of retrogradely labeled motoneurons compared with the contralateral PBS-treated side ($P < 0.002$), suggesting that VEGF can overcome the effects of disease on transport. (**D** and **E**) Twenty-four hours of TP treatment also induce a selective and significant deficit in endosomal flux ($P < 0.001$) in sciatic nerve axons, which exogenous VEGF prevents, suggesting that muscle-supplied VEGF can protect neuronal trafficking mechanisms from disease. Note that endosomal flux in WT controls was not affected by the VEGF treatment and that net velocity was neither affected by treatment nor genotype. Graphs represent mean ± SEM [(A) $N = 10$/group; (B) $N = 5$/group; (C) $N = 10$/group; (D, E) $N = 6$/group] and * indicates significant differences between groups based on PLSD *post hoc* tests of repeated measures ANOVA (A), PLSD *post hoc* tests of two-way ANOVA (B, D, E) and paired *t*-test (C). TP, testosterone propionate; PBS, phosphate-buffered saline; VEGF, vascular endothelial growth factor.

(Fig. 4D). While instantaneous velocity is unaffected in TG males, run length is significantly shortened ($P = 0.012$), with more endosomes stalling ($P = 0.036$) and more stalls per endosome ($P = 0.010$). In neither model was the frequency of reversals affected by disease.

Data on instantaneous velocity suggest that a major factor contributing to the reduction in net velocity of endosomes in diseased KI males is a reduction in instantaneous velocity, since both net and instantaneous velocity are reduced in KI males while neither are affected in diseased myogenic males. On the other hand, endosomal stalling may contribute to the flux deficit in both models. While reduced endosomal run length would be expected to also reduce net velocity in the myogenic model, it did not, possibly because so few (~15%) endosomes stall overall. Stall duration may also be a factor and contribute to the deficit in net velocity in KI males since stall time is twice as long in KIs compared with WTs [mean ± SEM: 24.53 ± 2.58 s (KI) versus 11.51 ± 7.57 s (WT)], whereas stall duration is equivalent in TG and WT males [21.64 ± 2.06 s (TG) vs. 19.58 ± 5.300 s (WT)]. On the other hand, diseased males in both models share other trafficking defects, namely a marked decrease in run length, reflecting the fact that more endosomes stall more often in diseased KI and TG males. The increased likelihood for endosomes to stall in diseased mice could potentially contribute to the flux deficit evident in both models with slowed endosomal movement adding further to the flux deficit in KI males. These disease-related changes in instantaneous velocity and run length suggest that function of the dynein/dynactin motor complex is affected in both the KI and myogenic models. Given where the disease-causing alleles are expressed in each model, these data implicate both cell autonomous and non-cell autonomous mechanisms in the regulation of mechanisms controlling efficient retrograde transport.

Retrograde labeling/trafficking defect emerges early and is reversed by VEGF

To explore the clinical relevance of our results, we investigated whether trafficking defects that arise early in the disease (presumably before the onset of secondary pathology) can be rescued with VEGF. Adult TG females are ideally suited for this purpose since disease is acutely triggered by androgen treatment. First, we repeated the analysis of grip strength and retrograde transport of CT-HRP in acutely diseased TG females, but at earlier time points to define the earliest detectable expression of disease. We find that 24 h after a single subcutaneous injection of T propionate (TP), both motor function and retrograde labeling of motoneurons are significantly reduced in TG females (Fig. 5A and B). This result suggests that disruption of axonal transport is indeed an early event in disease, and thus, could potentially underlie the motor symptoms.

We next examined whether this early deficit in transport could be reversed by treating muscles with exogenous VEGF, since disruption of VEGF signaling is implicated in other mouse models of SBMA (29) and VEGF mRNA is reduced in muscles of our myogenic-diseased TG males (20). We find that locally treating the AT muscle on one side of TG females

with recombinant (r)VEGF, in the face of systemic TP, protects against disease, significantly increasing the number of retrogradely labeled motoneurons on the rVEGF-treated side (Fig. 5C, $P = 0.0018$, paired *t*-test). Because only one muscle was briefly exposed to rVEGF, improvements in motor function were not assessed. To determine whether rVEGF can rescue the trafficking deficit in acutely diseased TG females, TG and WT female mice were treated systemically with TP and intramuscularly with VEGF, as above, with CT-AF_{488} co-injected into muscle with rVEGF or phosphate-buffered saline (PBS) 24 h later. We find that unilateral treatment with rVEGF selectively increases endosomal flux in sciatic nerve explants on only the rVEGF-treated side of diseased TG females (Fig. 5D, TG + rVEGF versus TG + PBS: $P < 0.0001$, paired *t*-test), thereby eliminating the flux deficit on that side compared with WT controls. As before, net velocity is normal in diseased females, and rVEGF has no effect on this measure in either TG or WT females (Fig. 5E). Thus, these data indicate that the effect of exogenous VEGF is specific, reversing a deficit in flux that is caused by disease, and suggest it may be therapeutically useful before the onset of secondary pathologies.

DISCUSSION

Defects in axonal transport are likely critical pathogenic events underlying the demise of neurons in disease (1,30). Non-cell autonomous mechanisms, mediated via cell–cell interactions, have also recently emerged as potent regulators of neuronal fate in disease (7). However, little direct attention has been given to whether defects in axonal transport are influenced by non-cell autonomous mechanisms. To address this issue, we examined retrograde labeling of motoneurons and retrograde trafficking of endosomes in living axons of diseased mice from two different SBMA mouse models, a KI model in which a polyQ-expanded *AR* allele is broadly expressed at normal levels (15), and a myogenic model in which a normal *AR* allele is strongly expressed only in skeletal muscle fibers (20). We find in each model that androgen-dependent motor dysfunction is accompanied by pronounced retrograde trafficking defects. Many fewer motoneurons in diseased mice are retrogradely labeled with CT-HRP, a deficit that at least in part reflects impairments in the efficiency by which CT-labeled endosomes are transported retrogradely along axons. Given where the disease allele is expressed in each model (broadly versus only skeletal muscle fibers), these data suggest retrograde trafficking mechanisms in motoneurons are subject to both cell and non-cell autonomous control. Because disease triggered in skeletal muscle imparts disease to motoneurons by perturbing retrograde axonal transport, skeletal muscles may be effective therapeutic targets for rescuing motoneurons from axonal transport dysfunction. Sensory neurons are also affected in SBMA (31), and may show comparable transport deficits, so muscles may also serve as a target for rescuing sensory neurons from disease.

Retrograde transport is impaired in living axons of SBMA diseased mice

We initially asked whether diseased mice in the KI and myogenic SMBA models showed impaired retrograde transport using the well-characterized neurotracer, CT-HRP. When injected into muscle, CT-HRP binds to ganglioside GM1 receptors in the plasma membrane of motor nerve terminals, triggering its uptake and retrograde transport to motoneuronal cell bodies (32). We found striking disease-related deficits in retrograde labeling of motoneurons in both models, although the deficit was more severe in KI males (Fig. 1). Given that mutant AR is expressed both in motoneurons and skeletal muscles of KI mice, these data provided the first hint that mutant AR may act via cell autonomous and non-cell autonomous mechanisms to perturb axonal transport.

However, other interpretations are possible. For example, fewer labeled motoneurons could reflect fewer total motoneurons, due to disease-induced cell death. We reported several findings that argue against this possibility. Counts of motoneurons through the rostrocaudal extent of AT motoneurons in spinal cords of affected KI males firmly establish that there is no motoneuronal loss in this model (Supplementary Material, Fig. S1). Moreover, although chronically diseased TG males have fewer or smaller motor axons (20,23), we found that castration of such males rescues both their motor function and retrograde axonal transport (Fig. 2A and B). We also found that doubling the transport time (from 12 to 24 h) eliminates the labeling deficit in acutely diseased TG females by increasing their number only in such females (Fig. 2C–E). Together, these findings argue that the labeling deficit does not reflect a deficit in the absolute number of motoneurons innervating the targeted muscle. Because the level of labeling in diseased females 'catches up' to that of controls when transport time is extended, diseased motoneurons appear to be slower to accumulate CT-HRP in their cell bodies after tracer is introduced into muscle, implicating defects in endocytotic and/or trafficking mechanisms. Monitoring endosomal trafficking directly in living axons confirmed this prediction.

To delineate possible mechanisms underlying this retrograde labeling deficit, we developed a method for live imaging of endosomal trafficking in sciatic nerve explants from SBMA mice. Endosomes were labeled via intramuscular injections of CT conjugated to AlexaFluor 488 (AF_{488}). Control experiments established that labeled endosomes were only evident in nerve explants after CT-AF_{488} was injected intramuscularly, that endosomal motility in nerve explants was microtubule-dependent and was stable in both healthy and diseased mice well beyond our standard 30 min recording window (Supplementary Material, Fig. S2). From these data, we conclude that our approach is a reliable and valid method for directly assessing the effects of disease on axonal transport/trafficking mechanisms, and offers distinct advantages over more commonly used methods, such as nerve ligation and cell culture.

We first examined the flux and net velocity of retrogradely transporting endosomes, as either could explain the slowed retrograde accumulation of CT-HRP in diseased motoneurons, yet each implicates different cellular mechanisms. For example, deficits in flux without effects on velocity implicate defects in endocytoctic mechanisms that regulate the uptake and early trafficking of endosomes. On the other hand, deficits in velocity implicate defects in trafficking mechanisms that underlie the long-range transport of cargo along axons, namely the dynein/dynactin motor protein complex.

Data from our trafficking studies provided direct evidence that retrograde axonal transport is impaired in both models. We found endosomal transport was more severely impaired in KI males than TG males, in accord with the greater deficit in retrograde CT-HRP labeling in the KIs. Specifically, while flux was significantly decreased in both models, the deficit was much larger in KI males than TG males (5-fold compared with 2-fold; see Fig. 3, Supplementary Material, Figs S3 and S4 and Movies S1 and S2). Moreover, net velocity was reduced only in KI males (Fig. 3). We also quantified instantaneous velocity and found it was reduced only in KI males (Fig. 4). These findings suggest that the deficit in net velocity exhibited only by KI males may largely reflect a deficit in the absolute speed at which endosomes are transported retrogradely in axons of diseased KI males.

We found, however, that other trafficking parameters were comparably impaired in both disease models. In particular, endosomes tend to stall more often in diseased axons of *both* models, resulting in reduced endosomal run lengths. This increased stalling behavior may contribute to the deficit in endosomal flux seen in both models. When endosomes stall more often, they are less likely to be moving, effectively reducing endosomal flux. However, endosomal flux reflects not only the efficiency by which endosomes are transported, but also other processes, including the rate of endosomal formation and endosomal size. While our data rule out any simple explanation of synaptic loss or reduced synaptic size on endosomal flux (Fig. 4), they do not rule out other potential contributing factors. Perhaps, steps in the endocytotic pathway are also perturbed, either slowing the rate at which endosomes are formed and/or reducing their size, limiting our ability to detect them. Both sorts of defects have been observed in a loss of function mutation linked to ALS2, a juvenile-onset form of ALS (33,34). The *ALS2* gene encodes for the protein alsin, which regulates rab5 activity, a key player in early vesicular trafficking, controlling the formation and retrograde trafficking of early endosomes. Moreover, given that mutant AR has also been shown to impair anterograde transport in cell model systems (17–18), it is also possible that the retrograde flux deficit is caused by impaired anterograde delivery of GM1 receptors to nerve terminals of diseased mice, which could decrease the amount of CT taken up for transport by motor axons. These findings direct attention to aspects of the early endocytotic pathway in SBMA.

Finding impaired transport efficiency in both SMBA models raises the intriguing possibility that some aspect of the dynein/dynactin motor complex is perturbed in both. One likely candidate is dynactin, given the role of dynactin in promoting efficient retrograde trafficking by lengthening the run length of dynein (3) and its implicated role in SBMA (6). Finding similar defects at the NMJ of diseased KI and TG males (increased synaptophysin staining and junctional fragmentation) as found in mice expressing mutant dynactin 1 (35,36) also points to perturbed dynactin function. However, other possibilities exist, including that mutant AR in motoneurons of KI males may indirectly impair retrograde transport by impairing anterograde transport. This is plausible, given that mutant AR can perturb anterograde transport in cell model systems (16–18) and the apparent dependence of retrograde transport on functional anterograde transport mechanisms (37). Whether anterograde transport is also disrupted in the KI or myogenic models of SBMA is currently unknown. It is also possible that decreased mitochondrial ATP contributes to the retrograde transport defect in the KI model since mitochondrial function is disrupted in this model (38). However, recent data indicating that retrograde transport of synaptic-related cargo is independent of mitochondrial ATP argues against this possibility (39). Because SBMA pathogenesis depends critically on activation of *nuclear* AR (21,40), it seems likely that altered transcriptional regulation of motor-associated proteins such as dynactin 1 plays a role in disrupting axonal transport in SBMA.

Previous evidence from the 97Q mouse model suggests that mutant AR acts in a cell autonomous manner to reduce the expression of dynactin 1, because only motoneurons containing misfolded AR protein showed reduced dynactin 1 expression and impaired retrograde labeling (6). However, we find significant endosomal stalling in diseased myogenic males, demonstrating that non-cell autonomous mechanisms can also regulate transport efficiency. One possibility is that muscle-derived neurotrophic factors binding to receptors in nerve terminals act to regulate the activity of the dynein/dynactin motor complex, possibly through some phosphorylation mechanism (41). Because CT appears to share the same pathways and membrane compartments as neurotrophic factors for retrograde transport (42,43), it is possible that our measures of endosomal trafficking (monitored by CT-AF_{488}) reflect not only changes in the trafficking of neurotrophic factors *per se*, but also their influence on dynein/dynactin function. The existing association between endosomal stalling and defects in neurotrophic factor expression in diseased muscles of both models (44) is consistent with this view.

While a great deal of attention is directed at understanding how neurotrophic factors are transported retrogradely (45), little attention has been given to how neurotrophic factors might regulate axonal transport *per se*. A notable exception is a single report showing that neurotrophic factors such as brain-derived neurotrophic factor (BDNF) injected into muscle reverse a disease-related deficit in retrograde labeling (22). How such neurotrophic factors work to rescue retrograde transport is unknown.

Neurotrophic factors as non-cell autonomous regulators of retrograde transport

Neurotrophic factors have recently gained renewed attention as potential therapies for treating neurodegenerative disease. A common theme of recent reports is the rescue of diseased neurons via indirect or non-cell autonomous routes, such as via the targets they innervate (46–49). However, whether neurotrophic factors rescue neurons from disease by providing necessary signals for survival and/or by reversing a transport defect is largely unexplored, despite precedence for both. Therefore, we asked whether defects in retrograde labeling/endosomal trafficking seen early in the disease process can be reversed by treating muscles with rVEGF. We chose to test VEGF because of the known deficit in this trophic factor in diseased TG muscles (20,44). TG females in the myogenic model were ideal for answering this question because disease occurs only when they are exposed to male levels of

androgens. Hence, we knew precisely when disease begins in TG females. We found that rVEGF injected into diseased muscles on one side greatly enhanced retrograde labeling of AT motoneurons on that side and prevented the disease-induced deficit in flux, while having no effect on net velocity nor affecting any trafficking measures in WT controls (Fig. 5). Thus, these results suggest that exogenous VEGF reverses the flux deficit by replenishing muscle-supplied VEGF, which ordinarily promotes the retrograde trafficking of endosomes. Because the KI and 97Q models of SBMA also show significant deficits in muscle VEGF (44), it is possible that transport dysfunction in motoneurons emerges because of a decreased supply of muscle-supplied VEGF and contributes to the loss of motor function in SBMA.

Recent evidence from a fourth TG mouse model suggests that defects in retrograde axonal transport may not be a pathogenic mechanism in SBMA (19). While it remains possible that axonal transport is unaffected by disease in this particular model, it is also possible that BDNF masked a genuine transport defect, since muscles of diseased and healthy mice were pretreated with BDNF before retrograde transport was assessed. Our finding that VEGF treatment enhances transport only in diseased motor axons without affecting retrograde transport in healthy axons raises this possibility.

A number of questions remain, including the mechanism of action by which rVEGF reverses the trafficking defect. Given that VEGF is retrogradely transported by motoneurons but also promotes synaptic stability (50), VEGF may rescue motoneurons from disease via both short- and long-range effects (51); it may act locally in the synapse to maintain early endocytotic and/or trafficking mechanisms, as well as acting upstream via retrograde transport in motoneuronal cell bodies, to possibly override the enhanced delivery of death signals (28). Moreover, how both the polyQ-expanded AR (expressed at normal levels) and the WT AR (expressed at high levels) cause androgen-dependent impairments in motor function and axonal transport is not clear, although recent data suggest that in both cases, AR toxicity arises via a common final pathway of abnormal amplification of native AR function (21). Our finding that over-expression of WT alleles engender comparable neuropathology as mutated alleles is not without precedence (52–54) and suggests that protein toxicity mediating disease [such as in ALS, Parkinson's, spinal cerebellar ataxia 1 (SCA1), and now SBMA] can arise via diverse pathways that may or may not involve changes in the amino acid sequence of the protein. The fact that only ~10% of ALS cases are familial supports this view. Indeed, recent data offer the surprising message that the polyglutamine expansion in ataxin 1 linked to SCA1 is neither sufficient nor necessary to cause disease (55,56). Because some 17% of male patients exhibit the same SBMA symptomatology (late-onset muscle wasting and weakness, along with gynaecomastia that indicates impaired AR function) but are found upon genetic screening to *lack* the expanded AR allele (57), different etiologies involving AR toxicity may lead to the same disorder. Nonetheless, if those different routes to the disorder all share a final common pathway, they may also all benefit from the same therapies. Because mice show striking androgen-dependent motor dysfunction when WT AR is over-expressed in skeletal muscle fibers, dysregulation of AR expression in muscle may be sufficient to cause SBMA in humans and could explain why some patients with SBMA symptoms do not carry an expanded allele of AR. Observations from the myogenic model also indicate that AR toxicity originating in muscle is sufficient to trigger distal axonopathy (20) and transport dysfunction in motoneurons, two disease traits common to many motoneuron diseases. In sum, our data along with other recently published data (15,46–48,58–62) underscore (1) the potential role of muscles in motoneuron disease and in particular, their role in perturbing retrograde transport, and (2) the potential therapeutic value of neurotrophic factors targeted to muscles and their motor synapses in the treatment of motoneuron diseases.

MATERIALS AND METHODS

SBMA mouse models

KI model. KI mice and age-matched WT controls maintained on a 129S1/SVLMJ background were obtained from our own breeding colony. They harbor a targeted CAG expanded allele of the first exon of the human *AR* gene as previously described (15). Mice used in these studies ranged in age from 90 to 160 days (mean age = 127 days), with each KI male matched to a WT control of the same age.

Myogenic model. TG mice expressing WT AR solely in skeletal muscle fibers were described previously (20). In brief, TG mice were generated carrying a cDNA encoding the rat *AR* gene under the control of the human skeletal α-actin (HSA) promoter. Of the lines produced, only those having relatively high levels of transgene expression exhibited a disease phenotype. TG male and female mice maintained on a C57Bl/J6 background from the symptomatic 141 line were used for the current studies, with TG males and age-matched WT controls exposed to prenatal flutamide as described below. Adult TG and WT females were age-matched and not exposed to flutamide prenatally. The age of mice used in these studies ranged in age from 90 to 120 days old.

All procedures involving mice were approved by Michigan State University Institutional Animal Care and Use Committee, and in accord with NIH guidelines for care and use of experimental animals. Isoflurane was used for all procedures requiring anesthesia.

Hormone manipulations

Prenatal flutamide rescue of TG males. More often than not, males carrying the HSA-AR transgene die on the day of birth (20). Many such males can be rescued from perinatal death by blocking the effects of prenatal testosterone with the AR antagonist, flutamide (20,23). Thus, timed pregnant TG dams were given daily subcutaneous (s.c.) injections of flutamide (5 mg flutamide dissolved in 100 μl in propylene glycol), on gestational days 14 through 21. Such flutamide-rescued TG males show an androgen-dependent disease phenotype comparable with TG male mice that survive postnatally without the aid of prenatal flutamide (23).

Castration of adult TG males. Adult (90-day-old) TG and WT brothers exposed prenatally to flutamide were gonadectomized under isoflurane anesthesia. Because such flutamide-rescued males have feminized anogenital distances and undescended testes as adults, gonads were removed via bilateral intraperitoneal incisions. Twenty-one days after gonadectomy, retrograde transport or trafficking was examined.

Hormone treatment of adult TG females. Females expressing the AR transgene in skeletal muscle fibers remain asymptomatic until exposed to adult male levels of testosterone (20). Thus, to induce disease, 90–120-day-old adult age-matched TG and WT female mice were ovariectomized under isoflurane anesthesia via two dorsolateral incisions just caudal to the rib cage and implanted with a Silastic capsule containing either crystalline testosterone (T; 1.57 mm inner diameter and 3.18 mm outer diameter, effective release length of 6 mm) or nothing (blank) s.c. at the nape of the neck just below the interscapular fat pad. Incisions were closed with sutures and wound clips. Such T implants result in serum T levels comparable with adult male mice (24). We find that it is only the combination of the AR transgene and male levels of T that leads to expression of disease in TG females. After 5 days of treatment, retrograde transport or trafficking was assessed as described below.

Acute T treatment. Retrograde transport/trafficking was also examined in a separate cohort of female mice after 24 h of acute T exposure. Because gonadectomy and/or hormone capsule implantation was found to transiently slow retrograde transport in both TG and WT females, acute T treatment was given via a single s.c. injection [1 mg of testosterone propionate (TP) in 50 μl of sesame oil or control injections of just oil]. Such females also received intramuscular injections of rVEGF or PBS vehicle. After twenty-four hours of treatment, retrograde transport or trafficking was assessed as described below.

Measures of motor dysfunction

Limb muscle strength was assessed based on the hang and grip strength tests as previously described (24). Male mice of the myogenic model were tested weekly starting at 21 days of age until sacrifice at 90–120 days, at which time either retrograde transport or trafficking was assessed. TG males show significant deficits in muscle strength compared with age-matched WT controls throughout this period. Because age of disease onset is highly variable in KI males (15), mice of this model were tested on the hang test every other day starting at 45 days. Retrograde transport or trafficking studies were done when hang times of KI males dropped to 60% of WT controls (age ranged from 90 to 160 days with a mean of 127 days of age).

To monitor changes in motor function after castration of TG males, performance on the hang and grip strength tests was assessed starting at 90 days of age (day 0), to obtain baseline muscle strength measures in TG and WT males just prior to surgical castration, and then on days 2, 4, 6, 8, 14 and 21 following castration, at which point axonal transport or trafficking was assessed. Only the data on hang test are reported for castrated males to facilitate direct comparison with gonadally intact TG and WT males, but grip strength measures also revealed robust recovery of motor function in TG males following castration. Forelimb grip strength was also used to monitor emergence of motor dysfunction in treated TG females, with baseline grip strength assessed in adult (90–120 days old) TG and age-matched WT females just prior to ovariectomy and capsule implantation (day 0) and then on days 1, 2, 3, 4 and 5 of treatment for the cohort in which retrograde transport was examined, and on 1, 3 and 5 days for the cohort in which axonal trafficking was examined. The effect of androgen on motor function in TG females is shown only for the cohort used to examine retrograde labeling of motoneurons, but the TG females examined for trafficking dysfunction also showed the same androgen-induced decline in motor function. Retrograde transport or axonal trafficking was assessed in females after 5 days of hormone or control treatment.

CT-HRP injection and histochemistry

To retrogradely label lumbar motoneurons, CT-HRP (1 μl of 0.2% CT-HRP/muscle; List Biological Labs, USA) was bilaterally injected into the AT muscle of anesthetized mice. After allowing CT-HRP 12 h to retrogradely transport to motoneuronal cell bodies (with the exception of one study in which labeling was assessed in TG and WT females after 24 h of transport), deeply anesthetized mice were perfused and their spinal cords processed for HRP histochemistry as described previously (63,64). One of two alternate series of sections was counterstained for Nissl substance using neutral red, allowing us to detect motoneurons that did not contain HRP. Estimates of the number of retrogradely labeled AT motoneurons were based on total bilateral counts done on adjacent sections using a 10× objective. Every lumbar section was examined for labeled motoneurons, including several sections beyond the rostral and caudal extent of AT motoneurons. While this counting method overestimates the number of labeled motoneurons (65), this error does not introduce spurious differences between experimental groups, given that motoneuron size is no different between diseased and healthy mice. In addition, estimates of the total number of motoneurons (with and without HRP) were based on unilateral counts done on the counterstained series of spinal cord section across the rostrocaudal extent of AT motoneurons (17 sections per mouse). Overall means are calculated with $N =$ number of animals/group and are reported in the figure captions unless noted in the results.

Sciatic nerve explant and labeling endosomes

Endosomal trafficking was examined in diseased and healthy mice in both the myogenic and KI models of SBMA adapting methods for monitoring trafficking endosomes in living axons of *Drosophila* and/or rodent sciatic nerve (25–27,66). Endosomes were visualized with cholera toxin B conjugated to Alexa Fluor 488 (CT-AF_{488}; Molecular Probes, USA, 10 μl of 0.2% in 0.9% saline containing 1% DMSO) that was injected into the AT and gastrocnemius muscles of isoflurane-anesthetized diseased and healthy mice. Retrograde movement of endosomes in living axons of explanted sciatic

nerves was monitored 4 h after injection. During the 4 h delay, mice were awake and mobile.

Mice were re-anesthetized to harvest the sciatic nerves, taking ~10 mm long segments just distal to the greater trochanter and just proximal to the small fat pad near the knee. Explants were placed on No. 1 cover glass (Corning, USA), maintaining their orientation as when dissected, glued in place (VetBond 3M, USA) and covered with 37°C oxygenated bicarbonate Ringer's solution (0.135 M NaCl, 0.005 M KCl, 0.001 M $MgCl_2$, 0.015 M $NaHCO_3$, 0.001 M Na_2PO_4, 0.002 M $CaCl_2$ and 0.011 M glucose, pH 7.2). The right sciatic nerve was harvested first and trafficking monitored, while the left nerve remained *in situ* in the anesthetized mouse. Body temperature was maintained using a heating pad for 30 min between nerve harvests. Once both nerves were harvested, the mouse was euthanized.

Live image acquisition and processing

Time-lapse movies of moving endosomes were made using an inverted LiveScan swept field confocal microscope (Nikon Eclipse TE2000-E, Japan) equipped with a 60× PlanApo oil immersion objective (1.4 na), illuminated with the 488 nm line of a 150 mW argon laser (Melles Griot) and recorded with a Photometrics CoolSNAP HQ^2 camera (USA) using the NIS elements software. Temperature of the sciatic nerve explant was maintained at 37°C by a ring incubator. Less than 10 min after nerve harvest, recordings began, with two time-lapse movies taken from the same explant within 30 min of harvest. Each movie was 7 min in length, comprising 211 images, with images captured every 2 s at a 1 s exposure. Laser power and aperture settings were identical for all captured images. Scanning for trafficking was started at the center of the sciatic nerve segment and proceeded toward the distal end of the nerve to reduce variability. Because of concerns about photobleaching, different axons in the same explants were used for the two movies and the second movie was taken from a region distal to the first. To minimize experimenter bias, video capture began when the first moving endosome could be kept in focus.

Trafficking measures from kymographs

Kymographs convert time-lapse movies into single images, which display trafficking endosomes moving along the length of an axon as a function of time. Trails of dotted lines represent trafficking endosomes in a single axon (Fig. 3A), which we refer to as 'endosomal traces'. Several trafficking measures were derived from kymographs, including net and instantaneous velocity, flux, stalls and reversals of retrogradely moving endosomes. Mean estimates of trafficking measures were based on 15–30 endosomal traces per kymograph, with 2–4 kymographs per mouse and $N =$ number of animals/group.

To make kymographs, the resulting movies were opened in NIH ImageJ as a 16 bit stack of images then rotated 90° counterclockwise. A 60 pixel wide length of axon was then cropped, and using the 're-slice' option, sliced into 1 pixel width sections and z-projected using the SUM option, which resulted in 32 bit 'raw' kymographs. The raw kymographs were converted to 16 bits, and saved as tiff files. To facilitate better visibility of transport events, raw kymographs were opened in Adobe Photoshop (7.0 or CS2; USA), color inverted and resampled to increase size by 500%, thus producing the kymographs used for analysis. Kymographs were analyzed in ImageJ.

Net velocity of retrogradely transported endosomes is the net distance traveled by endosomes in the distal to proximal direction over time and can include stalls, reversals in direction and/or changes in velocity. Measures of net velocity were obtained from kymographs by drawing a box around each endosomal trace such that the far ends of the trace pass through opposite corners of the box (as shown in Fig. 3A). Height and width of the box (in pixels) corresponding to length and time are used to calculate velocity (microns/second) based on the following formula: [Distance (pixels) × 0.10526 (microns/pixel)/Time (pixels) × seconds per frame]. Net velocities of individual endosomal traces in a single kymograph were then averaged to provide the mean net velocity/axon. These estimates were then averaged across individual axons sampled within a single animal to obtain a single estimate of net velocity per mouse.

Flux was determined by drawing a line through the center of the kymograph parallel to the time axis (as shown by the red line in Fig. 3A) and counting the number of endosomal traces which cross that line. The total number of endosomes per kymograph was then divided by 7 min (total time represented on the kymograph) to estimate endosomal flux in endosomes/minute. Such estimates were averaged across individual axons within a single animal to obtain a single estimate of flux per mouse.

Instantaneous velocity is an estimate of speed of endosomal transport absent of stalls or reversals. Instantaneous velocity was measured by drawing a one pixel wide line parallel to the time axis, bisecting the kymograph with respect to distance. For each endosomal trace crossing the center line, a 20 pixel box was drawn around it, centering it with respect to the bisecting line, with width and height of the box representing distance and time, respectively. The width of the box (20 pixels) accounted for 6.6% (1.67 μm) of the total distance traveled and any continuous velocity within it was considered instantaneous. The time it took to travel this short distance was calculated based on the height of the box, which was adjusted so that its corners intersected the most distal and proximal aspects of the trace. On rare occasions, perturbations in endosomal velocity, including changes in speed, stalls and/or reversals, appeared within the box. In such cases, the box was moved immediately distal to the trafficking perturbation or until the box included a part of the endosomal trace that contained no trafficking perturbations. Instantaneous velocity (microns/second) was calculated based on the same formula used for net velocity. Measures of instantaneous velocity for each endosome were averaged within a single kymograph and such estimates from two to four axons of the same mouse were averaged to obtain a single estimate of instantaneous velocity per mouse.

Stalls were defined as an endosome that was stationary for ≥2 s. Stalling prevalence was assessed by determining the number of stalls per endosomal trace and the proportion of

traces that had stalls. Average run length per animal was estimated by adding together the total distance of endosomal transport observed in a kymograph and dividing this by the number of stalls. As above, measures were averaged across multiple kymographs for each animal, with $N =$ no. of animals/group.

Nocodazole treatment and endosomal trafficking

Adult 50–60-day-old WT male mice were anesthetized with isoflurane and received intramuscular injections of nocodazole (25, 12.5 or 6.25 μg dissolved in DMSO; Sigma, USA) to disrupt microtubules, into the AT and gastrocnemius muscles, of one hindlimb. The same muscles of the other limb received control injections of DMSO. Ten hours later, 10 μl 0.2% CT-AF_{488} was injected bilaterally into each AT and gastrocnemius muscle. The side receiving nocodazole was alternated between mice. Four hours later, animals were re-anesthetized and explants of sciatic nerves were placed onto glass coverslips for live imaging of endosomal trafficking in axons as described above.

Visualization of NMJs

NMJs in the AT muscles of diseased and healthy mice were visualized with standard reagents [neurofilament and synaptophysin antibodies (myogenic model) or yellow fluorescent protein (YFP) (KI model) and tagged α-bungarotoxin]. The AT muscles were harvested from isoflurane-anesthetized age-matched adult (>120 days old) TG and WT males that were exposed to prenatal flutamide, pinned as flat whole mounts in Sylgard-coated dishes and fixed for 30 min in 4% paraformaldehyde followed by 3 h in phosphate-buffered (0.1 M, pH 7.4) 20% sucrose. Muscles were sectioned longitudinally at 60 μm on a freezing sliding microtome, rinsed in blocker (PBS containing 0.2% bovine serum albumin, 0.1% sodium azide and 0.3% triton X100) and incubated overnight at room temperature in rabbit anti-synaptophysin polyclonal antiserum (1:200; Zymed, 18–0130) and mouse anti-neurofilament monoclonal antiserum (2H3, 1:200, Developmental Studies Hybridoma Bank) rinsed in blocker and incubated for 2 h at room temperature in FITC conjugated secondary antisera, sheep anti-mouse (1:100; Sigma, E2266) and donkey anti-rabbit (1:100, Jackson Immunoresearch, 711.095.152) to visualize motor axons and their terminals and Alexa Fluor 555-labeled α-bungarotoxin (1:100; Invitrogen, B35451) to visualize postsynaptic junctions. The same procedures were used to examine NMJs in a separate cohort of age-matched adult TG and WT females given either T or blank capsules for 5 days. To examine NMJs in diseased KI males and age-matched controls, this line was crossed with TG mice obtained from Jackson Laboratories (strain: B6.Cg-Tg(Thy1-YFP)16Jrs/J; stock #: 003709) that expresses YFP in all motoneurons and their axons (67). Postsynaptic AChRs were visualized with AlexaFluor 647 conjugated alpha-bungarotoxin (1:100, Invitrogen, B35450). Twenty en face junctions were sampled across a muscle section per mouse, taking epifluorescent (myogenic model) or confocal (KI model) images of endplates which were thresholded and their area measured as previously described (68).

VEGF and retrograde transport/endosomal trafficking

Transport. Anesthetized 90–120-day-old age-matched TG female mice were injected s.c. just below the intrascapular fat pad with TP (1 mg in 50 μl sesame oil) and the AT muscle on one side was injected with 50 ng/1 μl mouse recombinant (r)VEGF (R&D Systems, USA) while 1 μl of vehicle (0.1 M, PBS) was injected into the other. Identical injections of VEGF and PBS were made 24 h later but co-injected with 1 μl 0.2% CT-HRP. Mice were perfused 12 h later and their spinal cords reacted for CT-HRP as described above. The cord was scored on the dorsal surface to mark the right side. The AT muscle that received VEGF was alternated between experimental mice to avoid any inherent asymmetries in transport.

Trafficking. To evaluate effects of rVEGF on endosomal trafficking, TG and WT females were injected with TP or the vehicle oil (as described above) and intramuscular injections of rVEGF (50 ng/muscle) into the AT and gastrocnemius on one side and PBS contralaterally. Muscles received the same rVEGF or PBS treatment 24 h later along with 10 μl 0.2% CT-AF_{488}. The side receiving rVEGF was alternated between experimental mice. Four hours after the last set of intramuscular injections, mice were re-anesthetized and sciatic nerve explants were mounted onto glass cover slips for endosomal trafficking studies as described above.

Statistics

T-tests (paired or unpaired, two-tailed) were used to determine significant differences between two groups. When the number of experimental groups exceeded two, significant differences between groups were determined based on an ANOVA design with *post hoc* comparisons using Fisher's protected least significant difference test (Statview, SAS, USA) with $P < 0.05$ taken as significant. Results are presented as group means (with $N =$ number of animals/group) ± standard error of the mean (SEM).

SUPPLEMENTARY MATERIAL

Supplementary Material is available at *HMG* online.

Conflict of Interest statement. None declared.

FUNDING

This work was supported by National Institute of Health grants NS045195 (C.L.J.) and NS055746 (A.P.L.), a Ruth L. Kirchstein National Research Service Award 1F32AR055848-01 (M.Q.K.) and a Ruth L. Kirchstein National Institutional Research Service Award T32-MH070343 (M.Q.K.), and startup funds from Michigan State University (K.E.M.).

REFERENCES

1. Perlson, E., Maday, S., Fu, M.M., Moughamian, A.J. and Holzbaur, E.L. (2010) Retrograde axonal transport: pathways to cell death? *Trends Neurosci.*, **33**, 335–344.
2. Morfini, G.A., Burns, M., Binder, L.I., Kanaan, N.M., LaPointe, N., Bosco, D.A., Brown, R.H. Jr, Brown, H., Tiwari, A., Hayward, L. *et al.* (2009) Axonal transport defects in neurodegenerative diseases. *J. Neurosci.*, **29**, 12776–12786.
3. King, S.J. and Schroer, T.A. (2000) Dynactin increases the processivity of the cytoplasmic dynein motor. *Nat. Cell Biol.*, **2**, 20–24.
4. Puls, I., Jonnakuty, C., LaMonte, B.H., Holzbaur, E.L., Tokito, M., Mann, E., Floeter, M.K., Bidus, K., Drayna, D., Oh, S.J. *et al.* (2003) Mutant dynactin in motor neuron disease. *Nat. Genet.*, **33**, 455–456.
5. Munch, C., Sedlmeier, R., Meyer, T., Homberg, V., Sperfeld, A.D., Kurt, A., Prudlo, J., Peraus, G., Hanemann, C.O., Stumm, G. *et al.* (2004) Point mutations of the p150 subunit of dynactin (DCTN1) gene in ALS. *Neurology*, **63**, 724–726.
6. Katsuno, M., Adachi, H., Minamiyama, M., Waza, M., Tokui, K., Banno, H., Suzuki, K., Onoda, Y., Tanaka, F., Doyu, M. *et al.* (2006) Reversible disruption of dynactin 1-mediated retrograde axonal transport in polyglutamine-induced motor neuron degeneration. *J. Neurosci.*, **26**, 12106–12117.
7. Ilieva, H., Polymenidou, M. and Cleveland, D.W. (2009) Non-cell autonomous toxicity in neurodegenerative disorders: ALS and beyond. *J. Cell Biol.*, **187**, 761–772.
8. Kennedy, W.R., Alter, M. and Sung, J.H. (1968) Progressive proximal spinal and bulbar muscular atrophy of late onset. A sex-linked recessive trait. *Neurology*, **18**, 671–680.
9. La Spada, A.R., Wilson, E.M., Lubahn, D.B., Harding, A.E. and Fischbeck, K.H. (1991) Androgen receptor gene mutations in X-linked spinal and bulbar muscular atrophy. *Nature*, **352**, 77–79.
10. Banno, H., Katsuno, M., Suzuki, K., Takeuchi, Y., Kawashima, M., Suga, N., Takamori, M., Ito, M., Nakamura, T., Matsuo, K. *et al.* (2009) Phase 2 trial of leuprorelin in patients with spinal and bulbar muscular atrophy. *Ann. Neurol.*, **65**, 140–150.
11. Takeyama, K., Ito, S., Yamamoto, A., Tanimoto, H., Furutani, T., Kanuka, H., Miura, M., Tabata, T. and Kato, S. (2002) Androgen-dependent neurodegeneration by polyglutamine-expanded human androgen receptor in Drosophila. *Neuron*, **35**, 855–864.
12. Montie, H.L. and Merry, D.E. (2009) Autophagy and access: understanding the role of androgen receptor subcellular localization in SBMA. *Autophagy*, **5**, 1194–1197.
13. Chevalier-Larsen, E.S., O'Brien, C.J., Wang, H., Jenkins, S.C., Holder, L., Lieberman, A.P. and Merry, D.E. (2004) Castration restores function and neurofilament alterations of aged symptomatic males in a transgenic mouse model of spinal and bulbar muscular atrophy. *J. Neurosci.*, **24**, 4778–4786.
14. Katsuno, M., Adachi, H., Kume, A., Li, M., Nakagomi, Y., Niwa, H., Sang, C., Kobayashi, Y., Doyu, M. and Sobue, G. (2002) Testosterone reduction prevents phenotypic expression in a transgenic mouse model of spinal and bulbar muscular atrophy. *Neuron*, **35**, 843–854.
15. Yu, Z., Dadgar, N., Albertelli, M., Gruis, K., Jordan, C., Robins, D.M. and Lieberman, A.P. (2006) Androgen-dependent pathology demonstrates myopathic contribution to the Kennedy disease phenotype in a mouse knock-in model. *J. Clin. Invest.*, **116**, 2663–2672.
16. Morfini, G., Pigino, G., Szebenyi, G., You, Y., Pollema, S. and Brady, S.T. (2006) JNK mediates pathogenic effects of polyglutamine-expanded androgen receptor on fast axonal transport. *Nat. Neurosci.*, **9**, 907–916.
17. Szebenyi, G., Morfini, G.A., Babcock, A., Gould, M., Selkoe, K., Stenoien, D.L., Young, M., Faber, P.W., MacDonald, M.E., McPhaul, M.J. *et al.* (2003) Neuropathogenic forms of huntingtin and androgen receptor inhibit fast axonal transport. *Neuron*, **40**, 41–52.
18. Piccioni, F., Pinton, P., Simeoni, S., Pozzi, P., Fascio, U., Vismara, G., Martini, L., Rizzuto, R. and Poletti, A. (2002) Androgen receptor with elongated polyglutamine tract forms aggregates that alter axonal trafficking and mitochondrial distribution in motor neuronal processes. *FASEB J.*, **16**, 1418–1420.
19. Malik, B., Nirmalananthan, N., Bilsland, L.G., La Spada, A.R., Hanna, M.G., Schiavo, G., Gallo, J.M. and Greensmith, L. (2011) Absence of disturbed axonal transport in spinal and bulbar muscular atrophy. *Hum. Mol. Genet.*, **20**, 1776–1786.
20. Monks, D.A., Johansen, J.A., Mo, K., Rao, P., Eagleson, B., Yu, Z., Lieberman, A.P., Breedlove, S.M. and Jordan, C.L. (2007) Overexpression of wild-type androgen receptor in muscle recapitulates polyglutamine disease. *Proc. Natl Acad. Sci. USA*, **104**, 18259–18264.
21. Nedelsky, N.B., Pennuto, M., Smith, R.B., Palazzolo, I., Moore, J., Nie, Z., Neale, G. and Taylor, J.P. (2010) Native functions of the androgen receptor are essential to pathogenesis in a Drosophila model of spinobulbar muscular atrophy. *Neuron*, **67**, 936–952.
22. Sagot, Y., Rosse, T., Vejsada, R., Perrelet, D. and Kato, A.C. (1998) Differential effects of neurotrophic factors on motoneuron retrograde labeling in a murine model of motoneuron disease. *J. Neurosci.*, **18**, 1132–1141.
23. Johansen, J.A., Troxell, S.M., Yu, Z., Mo, K., Monks, D.A., Lieberman, A.P., Breedlove, S.M. and Jordan, C.L. (2011) Prenatal flutamide enhances survival in a myogenic mouse model of spinal bulbar muscular atrophy. *Neurodegener. Dis.*, **8**, 25–34.
24. Johansen, J.A., Yu, Z., Mo, K., Monks, D.A., Lieberman, A.P., Breedlove, S.M. and Jordan, C.L. (2009) Recovery of function in a myogenic mouse model of spinal bulbar muscular atrophy. *Neurobiol. Dis.*, **34**, 113–120.
25. Misgeld, T., Kerschensteiner, M., Bareyre, F.M., Burgess, R.W. and Lichtman, J.W. (2007) Imaging axonal transport of mitochondria *in vivo*. *Nat. Methods*, **4**, 559–561.
26. Delcroix, J.D., Valletta, J.S., Wu, C., Hunt, S.J., Kowal, A.S. and Mobley, W.C. (2003) NGF signaling in sensory neurons: evidence that early endosomes carry NGF retrograde signals. *Neuron*, **39**, 69–84.
27. Viancour, T.A. and Kreiter, N.A. (1993) Vesicular fast axonal transport rates in young and old rat axons. *Brain Res.*, **628**, 209–217.
28. Perlson, E., Jeong, G.B., Ross, J.L., Dixit, R., Wallace, K.E., Kalb, R.G. and Holzbaur, E.L. (2009) A switch in retrograde signaling from survival to stress in rapid-onset neurodegeneration. *J. Neurosci.*, **29**, 9903–9917.
29. Sopher, B.L., Thomas, P.S. Jr, LaFevre-Bernt, M.A., Holm, I.E., Wilke, S.A., Ware, C.B., Jin, L.W., Libby, R.T., Ellerby, L.M. and La Spada, A.R. (2004) Androgen receptor YAC transgenic mice recapitulate SBMA motor neuronopathy and implicate VEGF164 in the motor neuron degeneration. *Neuron*, **41**, 687–699.
30. Brady, S. and Morfini, G. (2010) A perspective on neuronal cell death signaling and neurodegeneration. *Mol. Neurobiol.*, **42**, 25–31.
31. Suzuki, K., Katsuno, M., Banno, H., Takeuchi, Y., Atsuta, N., Ito, M., Watanabe, H., Yamashita, F., Hori, N., Nakamura, T. *et al.* (2008) CAG repeat size correlates to electrophysiological motor and sensory phenotypes in SBMA. *Brain*, **131**, 229–239.
32. Roux, S., Colasante, C., Saint Cloment, C., Barbier, J., Curie, T., Girard, E., Molgo, J. and Brulet, P. (2005) Internalization of a GFP-tetanus toxin C-terminal fragment fusion protein at mature mouse neuromuscular junctions. *Mol. Cell Neurosci.*, **30**, 79–89.
33. Devon, R.S., Orban, P.C., Gerrow, K., Barbieri, M.A., Schwab, C., Cao, L.P., Helm, J.R., Bissada, N., Cruz-Aguado, R., Davidson, T.L. *et al.* (2006) Als2-deficient mice exhibit disturbances in endosome trafficking associated with motor behavioral abnormalities. *Proc. Natl Acad. Sci. USA*, **103**, 9595–9600.
34. Jacquier, A., Buhler, E., Schafer, M.K., Bohl, D., Blanchard, S., Beclin, C. and Haase, G. (2006) Alsin/Rac1 signaling controls survival and growth of spinal motoneurons. *Ann. Neurol.*, **60**, 105–117.
35. Chevalier-Larsen, E.S., Wallace, K.E., Pennise, C.R. and Holzbaur, E.L. (2008) Lysosomal proliferation and distal degeneration in motor neurons expressing the G59S mutation in the p150Glued subunit of dynactin. *Hum. Mol. Genet.*, **17**, 1946–1955.
36. Lai, C., Lin, X., Chandran, J., Shim, H., Yang, W.J. and Cai, H. (2007) The G59S mutation in p150(glued) causes dysfunction of dynactin in mice. *J. Neurosci.*, **27**, 13982–13990.
37. Martin, M., Iyadurai, S.J., Gassman, A., Gindhart, J.G. Jr, Hays, T.S. and Saxton, W.M. (1999) Cytoplasmic dynein, the dynactin complex, and kinesin are interdependent and essential for fast axonal transport. *Mol. Biol. Cell*, **10**, 3717–3728.
38. Ranganathan, S., Harmison, G.G., Meyertholen, K., Pennuto, M., Burnett, B.G. and Fischbeck, K.H. (2009) Mitochondrial abnormalities in spinal and bulbar muscular atrophy. *Hum. Mol. Genet.*, **18**, 27–42.
39. Baqri, R.M., Turner, B.A., Rheuben, M.B., Hammond, B.D., Kaguni, L.S. and Miller, K.E. (2009) Disruption of mitochondrial DNA replication in Drosophila increases mitochondrial fast axonal transport in vivo. *PLoS ONE*, **4**, e7874.
40. Montie, H.L., Cho, M.S., Holder, L., Tsvetkov, A.S., Finkbeiner, S. and Merry, D.E. (2009) Cytoplasmic retention of polyglutamine-expanded

androgen receptor ameliorates disease via autophagy in a mouse model of spinal and bulbar muscular atrophy. *Hum. Mol. Genet.*, **18**, 1937–1950.
41. Ou, C.Y., Poon, V.Y., Maeder, C.I., Watanabe, S., Lehrman, E.K., Fu, A.K., Park, M., Fu, W.Y., Jorgensen, E.M., Ip, N.Y. *et al.* (2010) Two cyclin-dependent kinase pathways are essential for polarized trafficking of presynaptic components. *Cell*, **141**, 846–858.
42. Bronfman, F.C., Tcherpakov, M., Jovin, T.M. and Fainzilber, M. (2003) Ligand-induced internalization of the p75 neurotrophin receptor: a slow route to the signaling endosome. *J. Neurosci.*, **23**, 3209–3220.
43. Bronfman, F.C., Escudero, C.A., Weis, J. and Kruttgen, A. (2007) Endosomal transport of neurotrophins: roles in signaling and neurodegenerative diseases. *Dev. Neurobiol.*, **67**, 1183–1203.
44. Mo, K., Razak, Z., Rao, P., Yu, Z., Adachi, H., Katsuno, M., Sobue, G., Lieberman, A.P., Westwood, J.T. and Monks, D.A. (2010) Microarray analysis of gene expression by skeletal muscle of three mouse models of Kennedy disease/spinal bulbar muscular atrophy. *PLoS ONE*, **5**, e12922.
45. Cosker, K.E., Courchesne, S.L. and Segal, R.A. (2008) Action in the axon: generation and transport of signaling endosomes. *Curr. Opin. Neurobiol.*, **18**, 270–275.
46. Palazzolo, I., Stack, C., Kong, L., Musaro, A., Adachi, H., Katsuno, M., Sobue, G., Taylor, J.P., Sumner, C.J., Fischbeck, K.H. *et al.* (2009) Overexpression of IGF-1 in muscle attenuates disease in a mouse model of spinal and bulbar muscular atrophy. *Neuron*, **63**, 316–328.
47. Dobrowolny, G., Giacinti, C., Pelosi, L., Nicoletti, C., Winn, N., Barberi, L., Molinaro, M., Rosenthal, N. and Musaro, A. (2005) Muscle expression of a local Igf-1 isoform protects motor neurons in an ALS mouse model. *J. Cell Biol.*, **168**, 193–199.
48. Li, W., Brakefield, D., Pan, Y., Hunter, D., Myckatyn, T.M. and Parsadanian, A. (2007) Muscle-derived but not centrally derived transgene GDNF is neuroprotective in G93A-SOD1 mouse model of ALS. *Exp. Neurol.*, **203**, 457–471.
49. Ciriza, J., Moreno-Igoa, M., Calvo, A.C., Yague, G., Palacio, J., Miana-Mena, F.J., Munoz, M.J., Zaragoza, P., Brulet, P. and Osta, R. (2008) A genetic fusion GDNF-C fragment of tetanus toxin prolongs survival in a symptomatic mouse ALS model. *Restor. Neurol. Neurosci.*, **26**, 459–465.
50. Storkebaum, E., Lambrechts, D., Dewerchin, M., Moreno-Murciano, M.P., Appelmans, S., Oh, H., Van Damme, P., Rutten, B., Man, W.Y., De Mol, M. *et al.* (2005) Treatment of motoneuron degeneration by intracerebroventricular delivery of VEGF in a rat model of ALS. *Nat. Neurosci.*, **8**, 85–92.
51. Sondell, M., Sundler, F. and Kanje, M. (2000) Vascular endothelial growth factor is a neurotrophic factor which stimulates axonal outgrowth through the flk-1 receptor. *Eur. J. Neurosci.*, **12**, 4243–4254.
52. Singleton, A.B., Farrer, M., Johnson, J., Singleton, A., Hague, S., Kachergus, J., Hulihan, M., Peuralinna, T., Dutra, A., Nussbaum, R. *et al.* (2003) alpha-Synuclein locus triplication causes Parkinson's disease. *Science*, **302**, 841.
53. Jaarsma, D., Haasdijk, E.D., Grashorn, J.A., Hawkins, R., van Duijn, W., Verspaget, H.W., London, J. and Holstege, J.C. (2000) Human Cu/Zn superoxide dismutase (SOD1) overexpression in mice causes mitochondrial vacuolization, axonal degeneration, and premature motoneuron death and accelerates motoneuron disease in mice expressing a familial amyotrophic lateral sclerosis mutant SOD1. *Neurobiol. Dis.*, **7**, 623–643.
54. Fernandez-Funez, P., Nino-Rosales, M.L., de Gouyon, B., She, W.C., Luchak, J.M., Martinez, P., Turiegano, E., Benito, J., Capovilla, M., Skinner, P.J. *et al.* (2000) Identification of genes that modify ataxin-1-induced neurodegeneration. *Nature*, **408**, 101–106.
55. Duvick, L., Barnes, J., Ebner, B., Agrawal, S., Andresen, M., Lim, J., Giesler, G.J., Zoghbi, H.Y. and Orr, H.T. (2010) SCA1-like disease in mice expressing wild-type ataxin-1 with a serine to aspartic acid replacement at residue 776. *Neuron*, **67**, 929–935.
56. Emamian, E.S., Kaytor, M.D., Duvick, L.A., Zu, T., Tousey, S.K., Zoghbi, H.Y., Clark, H.B. and Orr, H.T. (2003) Serine 776 of ataxin-1 is critical for polyglutamine-induced disease in SCA1 transgenic mice. *Neuron*, **38**, 375–387.
57. Mariotti, C., Castellotti, B., Pareyson, D., Testa, D., Eoli, M., Antozzi, C., Silani, V., Marconi, R., Tezzon, F., Siciliano, G. *et al.* (2000) Phenotypic manifestations associated with CAG-repeat expansion in the androgen receptor gene in male patients and heterozygous females: a clinical and molecular study of 30 families. *Neuromuscul. Disord.*, **10**, 391–397.
58. Wong, M. and Martin, L.J. (2010) Skeletal muscle-restricted expression of human SOD1 causes motor neuron degeneration in transgenic mice. *Hum. Mol. Genet.*, **19**, 2284–2302.
59. Wang, L.J., Lu, Y.Y., Muramatsu, S., Ikeguchi, K., Fujimoto, K., Okada, T., Mizukami, H., Matsushita, T., Hanazono, Y., Kume, A. *et al.* (2002) Neuroprotective effects of glial cell line-derived neurotrophic factor mediated by an adeno-associated virus vector in a transgenic animal model of amyotrophic lateral sclerosis. *J. Neurosci.*, **22**, 6920–6928.
60. Mohajeri, M.H., Figlewicz, D.A. and Bohn, M.C. (1999) Intramuscular grafts of myoblasts genetically modified to secrete glial cell line-derived neurotrophic factor prevent motoneuron loss and disease progression in a mouse model of familial amyotrophic lateral sclerosis. *Hum. Gene Ther.*, **10**, 1853–1866.
61. Riddoch-Contreras, J., Yang, S.Y., Dick, J.R., Goldspink, G., Orrell, R.W. and Greensmith, L. (2009) Mechano-growth factor, an IGF-I splice variant, rescues motoneurons and improves muscle function in SOD1(G93A) mice. *Exp. Neurol.*, **215**, 281–289.
62. Azzouz, M., Ralph, G.S., Storkebaum, E., Walmsley, L.E., Mitrophanous, K.A., Kingsman, S.M., Carmeliet, P. and Mazarakis, N.D. (2004) VEGF delivery with retrogradely transported lentivector prolongs survival in a mouse ALS model. *Nature*, **429**, 413–417.
63. Park, J.J., Zup, S.L., Verhovshek, T., Sengelaub, D.R. and Forger, N.G. (2002) Castration reduces motoneuron soma size but not dendritic length in the spinal nucleus of the bulbocavernosus of wild-type and BCL-2 overexpressing mice. *J. Neurobiol.*, **53**, 403–412.
64. Zuloaga, D.G., Morris, J.A., Monks, D.A., Breedlove, S.M. and Jordan, C.L. (2007) Androgen-sensitivity of somata and dendrites of spinal nucleus of the bulbocavernosus (SNB) motoneurons in male C57BL6J mice. *Horm. Behav.*, **51**, 207–212.
65. Konigsmark, B.W. (1970) In Nauta, W.J.H. and Ebbeson, S.O.E. (eds), *Contempory Research Methods in Neuroanatomy*. Springer-Verlag, New York, pp. 315–340.
66. Miller, K.E., DeProto, J., Kaufmann, N., Patel, B.N., Duckworth, A. and Van Vactor, D. (2005) Direct observation demonstrates that Liprin-alpha is required for trafficking of synaptic vesicles. *Curr. Biol.*, **15**, 684–689.
67. Feng, G., Mellor, R.H., Bernstein, M., Keller-Peck, C., Nguyen, Q.T., Wallace, M., Nerbonne, J.M., Lichtman, J.W. and Sanes, J.R. (2000) Imaging neuronal subsets in transgenic mice expressing multiple spectral variants of GFP. *Neuron*, **28**, 41–51.
68. Jordan, C.L. and Williams, T.J. (2001) Testosterone regulates terminal Schwann cell number and junctional size during developmental synapse elimination. *Dev. Neurosci.*, **23**, 441–451.

Supplemental data

Figure S1 Diseased knock-in (KI) males have as many motoneurons as wild-type (WT) males based on Nissl staining despite marked deficits in retrograde labeling. Twelve hours after CT-HRP was injected into the anterior tibilias (AT), spinal cord cross sections were reacted for HRP, and one of two alternate series of sections from each spinal cord were counterstained with neutral red before coverslipping. Note that many motoneurons in diseased KI males stain red (black arrow) but do not contain black CT-HRP reaction product. Counts of the number of Nissl-stained motoneurons spanning the rostrocaudal extent of AT motoneurons confirm that KI and WT males have comparable numbers of motoneurons in the lower lumbar cord (WT: 224 $\pm$ 22.4 (mean $\pm$ SEM) versus KI: 275 $\pm$ 18.5) and suggest that AT motoneurons are present in diseased KI males but fail to efficiently take-up and/or retrogradely transport CT-HRP.

Figure S2 Retrograde trafficking of CT-AF_{488} labeled endosomes in sciatic nerve explants is stable and microtubule-dependent. (A-B) Videos taken from the same nerve explants of wild-type (WT) or transgenic (TG) male mice over time indicate that endosomal trafficking is stable for at least 40 minutes after nerves are dissected from mice, with no evidence of a fall-off in either the speed (velocity) or the number (flux) of CT-labeled endosomes that traffic retrogradely in explanted sciatic nerve. Given that endosomal trafficking in diseased axons appears no more susceptible to deterioration than in axons from healthy mice, the deficit in flux (B) detected *ex vivo* is likely also present in axons *in vivo*. That net velocity of transported endosomes is apparently *un*affected and stable in nerves from TG males also reinforces this view. (C-D) Pretreatment of AT and gastrocnemius muscles with nocodazole (6.25 µg/muscle) 10 hrs before intramuscular injections of CT-AF_{488} significantly reduces both net velocity (C) and flux (D) of

retrogradely trafficking endosomes compared to contralateral control-treated nerves from the same WT male mice, demonstrating that retrograde trafficking of CT-AF_{488} labeled endosomes is microtubule-dependent. Doubling the dose of nocodazole (12.5 μg/muscle) resulted in endosomes moving in an oscillating pattern with little net retrograde movement whereas 25 μg nocodazole/muscle completely blocked all endosomal trafficking. A, B: N = 6/group for the first two videos with N = 2-3 for video 3. C, D: * $p < 0.04$, based on a paired T-tests with N = 4/group.

Figure S3 Representative kymographs showing impaired retrograde transport of fluorescently labeled endosomes in sciatic nerve axons of diseased KI and TG males. While axons in both disease models exhibit deficits in flux (exemplified by the fewer number of endosomal traces in the kymographs from KI and TG males compared to WT controls, also see Fig 3B, D), the depletion of endosomes in KI males is much more severe. Endosomes in axons of KI males also tend to move more slowly (exemplified by the reduced slope of many endosomal traces) compared to WT males. This reduced instantaneous velocity (also see Fig 4C) may explain the decrease in net velocity seen in this model (Fig 3C). Endosomes in both disease models stall more often (black arrows), effectively shortening the average run length of endosomes (Fig 4C, D). Given that both models express a disease-causing AR allele in muscle, these data raise the possibility that disease originating in muscle can impair dynactin function independent of disease originating in motoneurons.

Figure S4 Endosomal flux and net velocity are comparable during the two videos taken consecutively from the same set of nerve explants (A – D). Less than 10 minutes after nerve

harvest, recordings began, with two time-lapse movies taken from the same explant within thirty minutes of harvest. Each of two movies was 7 minutes in length, with no more than 2.2 minutes delay on average between videos. These data argue that the deficits in endosomal flux exhibited by both diseased models (see also Figure 3B, D) and the deficit in net velocity seen only in the KI model (see also Figure 3C) reflect genuine trafficking defects *in vivo*.

Supplemental Movies

Movie S1-S2. Movies showing impaired retrograde transport of endosomes labeled with CT-AF_{488} in axons of sciatic nerve explants from diseased males of two different mouse models of SBMA (related to Figure 4), a knock-in (KI) model (S1) and a myogenic transgenic (TG) model (S2). Endosomal transport in affected TG males (S1) exhibit a deficit in flux (endosomes/min) compared to WT controls without effects on velocity, whereas KI males (S2) exhibit deficits in both flux and velocity (microns/sec). Time-lapse movies of moving endosomes were made using an inverted confocal microscope (Nikon Eclipse TE2000-E, Japan) equipped with a PlanApo 60X oil objective (NA 1.4), 488 nm laser (PraireView, USA) and a Photometrics CoolSNAP HQ^2 camera (USA). Each movie is 7 minutes in length, comprising 211 images, with images captured every 2 sec at a 1 sec exposure. Scale bar = 5 μm.

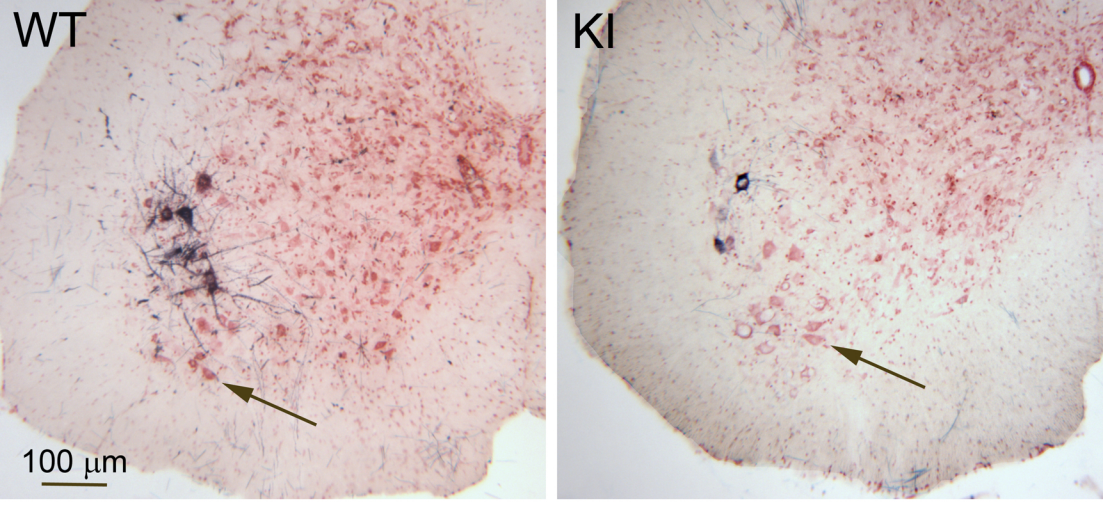

Sup. Fig. 1

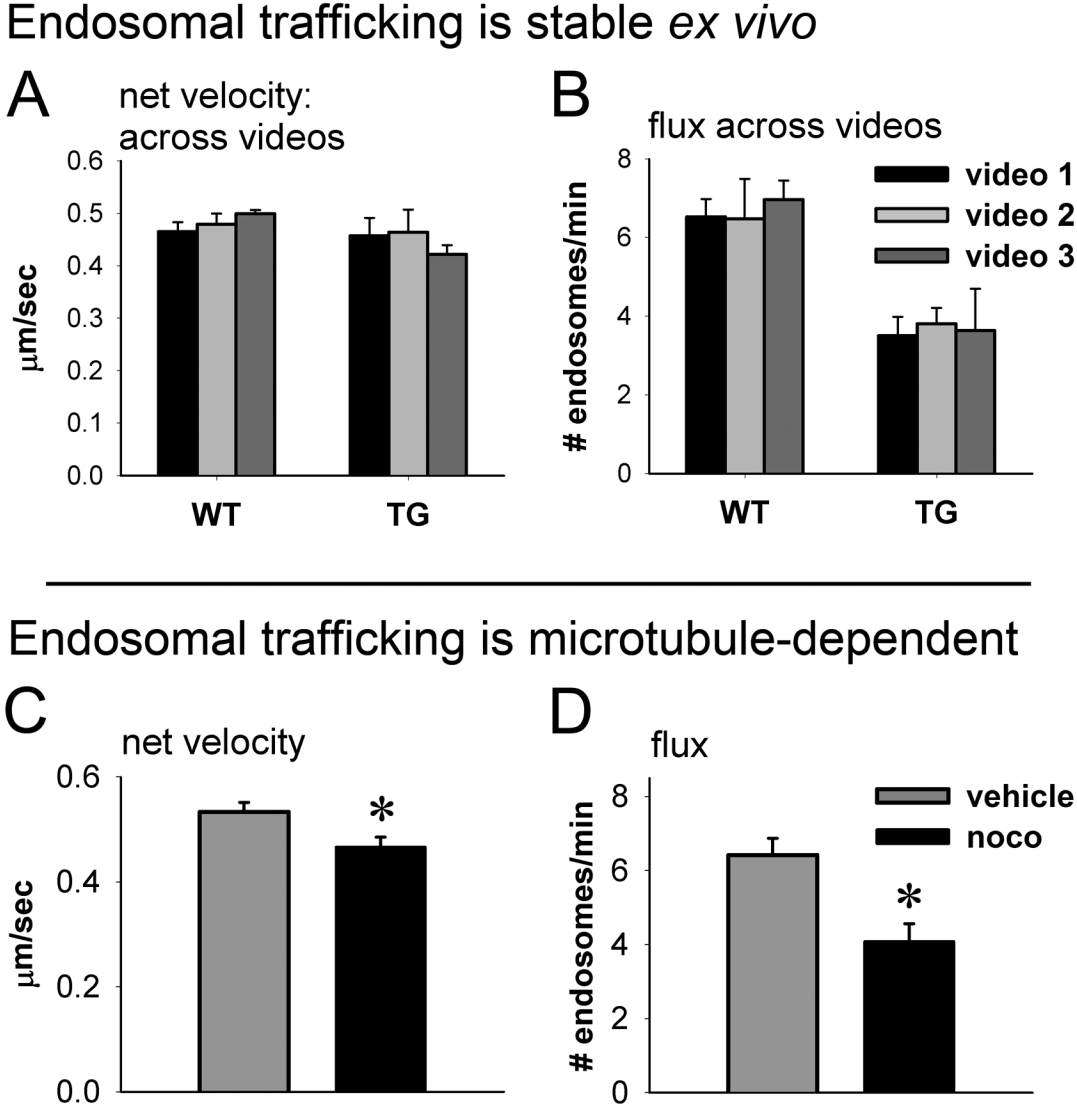
Endosomal trafficking is stable ex vivo
A
net velocity:
across videos
μm/sec
0.6
0.5
0.4
0.3
0.2
0.1
0.0
WT
TG
B
flux across videos
endosomes/min
8
6
4
2
0
video 1
video 2
video 3
WT
TG
Endosomal trafficking is microtubule-dependent
C
net velocity
μm/sec
0.6
0.4
0.2
0.0
*
D
flux
endosomes/min
8
6
4
2
0
vehicle
noco
*

Sup. Fig. 2

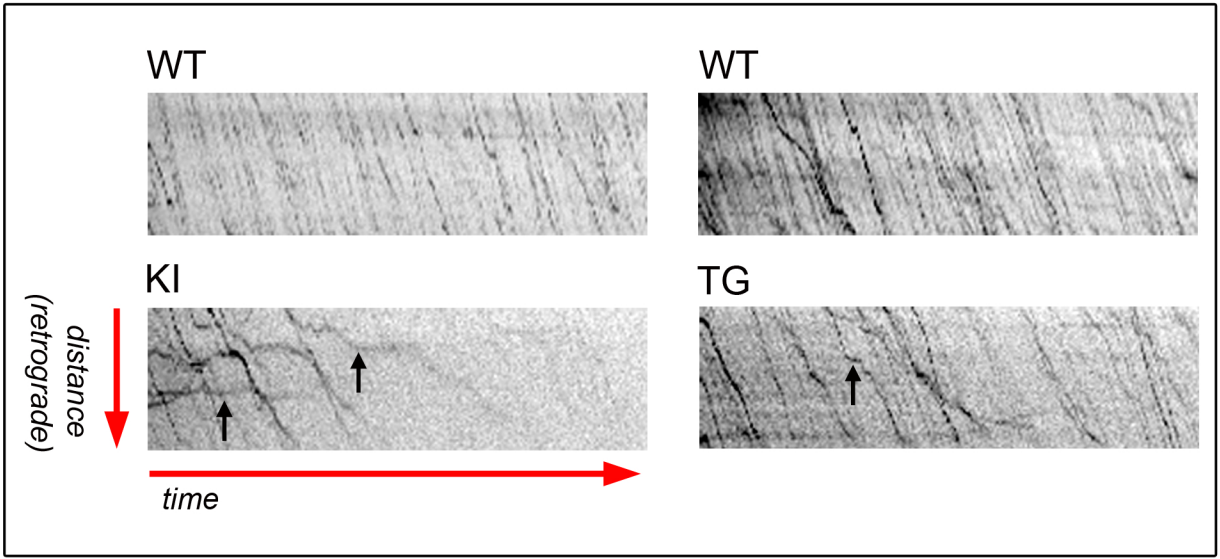

Sup. Fig. 3

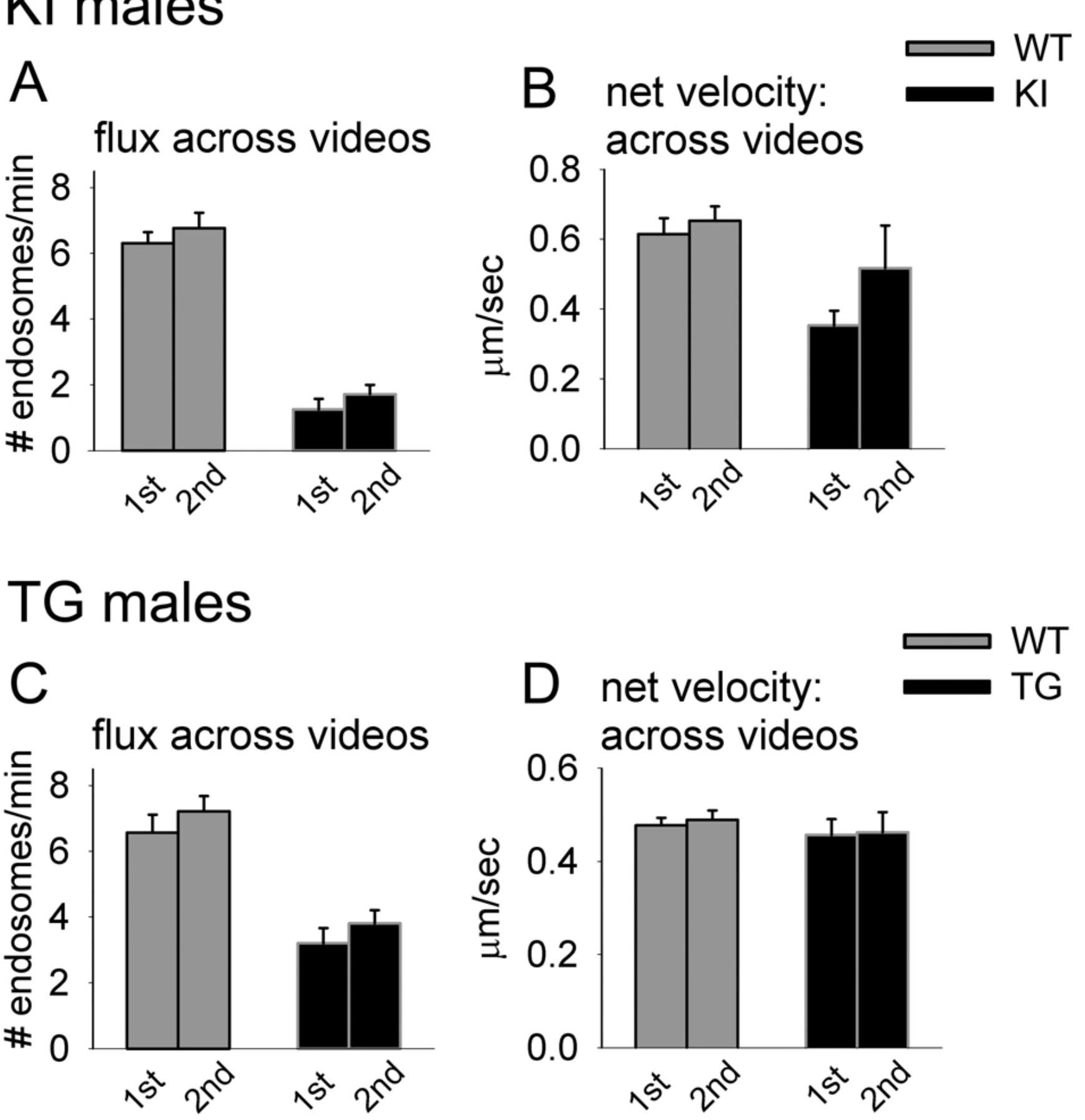
KI males
A
flux across videos
endosomes/min
0
2
4
6
8
1st
2nd
1st
2nd
B
net velocity:
across videos
µm/sec
0.0
0.2
0.4
0.6
0.8
1st
2nd
1st
2nd
WT
KI
TG males
C
flux across videos
endosomes/min
0
2
4
6
8
1st
2nd
1st
2nd
D
net velocity:
across videos
µm/sec
0.0
0.2
0.4
0.6
1st
2nd
1st
2nd
WT
TG

Sup. Fig. 4